Chapter 7

Balanced flow

In Chapter 6 we derived the equations that govern the evolution of the atmosphere and ocean, setting our discussion on a sound theoretical footing. However, these equations describe myriad phenomena, many of which are not central to our discussion of the large-scale circulation of the atmosphere and ocean. In this chapter, therefore, we focus on a subset of possible motions known as 'balanced flows' which are relevant to the general circulation.

We have already seen that large-scale flow in the atmosphere and ocean is hydrostatically balanced in the vertical in the sense that gravitational and pressure gradient forces balance one another, rather than inducing accelerations. It turns out that the atmosphere and ocean are also close to balance in the horizontal, in the sense that Coriolis forces are balanced by horizontal pressure gradients in what is known as 'geostrophic motion' — from the Greek: 'geo' for 'earth', 'strophe' for 'turning'. In this Chapter we describe how the rather peculiar and counter-intuitive properties of the geostrophic motion of a homogeneous fluid are encapsulated in the 'Taylor-Proudman theorem' which expresses in mathematical form the 'stiffness' imparted to a fluid by rotation. This stiffness property will be repeatedly applied in later chapters to come to some understanding of the large-scale circulation of the atmosphere and ocean. We go on to discuss how the Taylor-Proudman theorem is modified in a fluid in which the density is not homogeneous but varies from place to place, deriving the 'thermal wind equation'. Finally we discuss so-called 'ageostrophic flow' motion, which is not in geostrophic balance but is modified by friction in regions where the atmosphere and ocean rubs against solid boundaries or at the atmosphere-ocean interface.

7.1 Geostrophic motion

Let us begin with the momentum equation (6.43) for a fluid on a rotating Earth and consider the magnitude of the various terms. First, we restrict attention to the free atmosphere and ocean (by which we mean away from boundary layers), where friction is negligible[1]. Suppose each of the horizontal flow components u and v has a typical magnitude $\mathcal{U}$, and that each varies in time with a characteristic time scale $\mathcal{T}$ and with horizontal position over a characteristic length scale L. Then the first two terms on the left side of the horizontal components of Eq.(6.43) scale as[2]:

$$\underset{}{\frac{D\mathbf{u}}{Dt}} + \underset{}{f\widehat{\mathbf{z}}\times\mathbf{u}} = \underset{\frac{\mathcal{U}}{\mathcal{T}}}{\frac{\partial\mathbf{u}}{\partial t}} + \underset{\frac{\mathcal{U}^2}{L}}{\mathbf{u}\cdot\nabla\mathbf{u}} + \underset{f\mathcal{U}}{f\widehat{\mathbf{z}}\times\mathbf{u}}$$

For typical large scale flows in the atmosphere, $\mathcal{U}\sim 10\,\mathrm{m\,s^{-1}}$, $L\sim 10^6\,\mathrm{m}$, and $\mathcal{T}\sim 10^5\,\mathrm{s}$ and so $\mathcal{U}/\mathcal{T}\approx\mathcal{U}^2/L\sim 10^{-4}\,\mathrm{m\,s^{-2}}$. That $\mathcal{U}/\mathcal{T}\approx\mathcal{U}^2/L$ is no accident; the time scale on which motions change is intimately related to the time taken for the flow to traverse a distance L, *viz.*, $L/\mathcal{U}$. So in practice the acceleration terms $\frac{\partial\mathbf{u}}{\partial t}$ and $\mathbf{u}\cdot\nabla\mathbf{u}$ are of comparable in magnitude to one-another and scale like $\mathcal{U}^2/L$. The ratio of these acceleration terms to the Coriolis term is known as the *Rossby number*[3]:

[1] The effects of molecular viscosity are utterly negligible in the atmosphere and ocean, except very close to solid boundaries. Small-scale turbulent motions can in some ways act like viscosity, with an 'effective eddy viscosity' that is much larger than the molecular value. However, even these effects are usually quite negligible away from the boundaries.

[2] We have actually anticipated something here that is evident only *a posteriori*: vertical advection makes a negligible contribution to $(\mathbf{u}\cdot\nabla)\,\mathbf{u}$.

[3] Carl-Gustav Rossby (1898-1957). Swedish-born meteorologist, one of the major figures in the founding of modern dynamical study of the atmosphere and ocean. In 1928, he was appointed chair of meteorology in the Department of Aeronautics in 1928 at M.I.T. This group later developed into the first Department of Meteorology in an academic institution in the United States. His name is recalled ubiquitously in Rossby

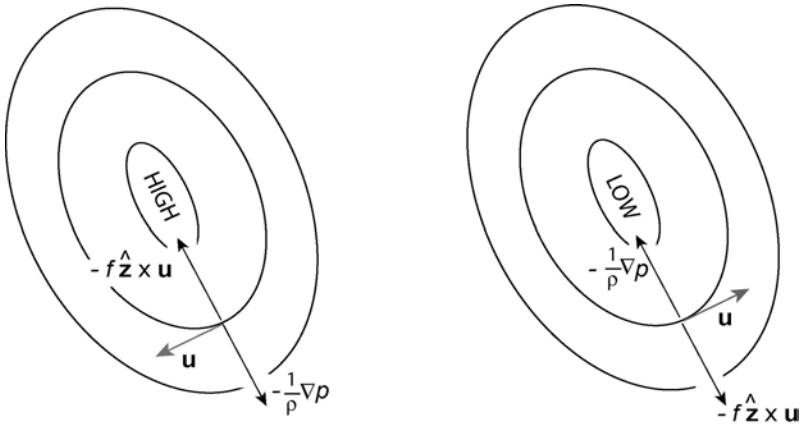

Figure 7.1: Geostrophic flow around (left) a high pressure center and (right) a low pressure center. (Northern hemisphere case, $f > 0$.) The effect of Coriolis deflecting flow 'to the right' — see Fig.6.10 — is balanced by the horizontal component of the pressure gradient force, $-\frac{1}{\rho}\nabla p$, directed from high to low pressure.

$$R_o = \frac{\mathcal{U}}{fL} \tag{7.1}$$

In middle latitudes (say near 45° — see Table 6.1), $f \simeq 2\Omega/\sqrt{2} = 1.03 \times 10^{-4}\,\mathrm{s}^{-1}$. So, given our typical numbers, $R_o \simeq 0.1$: the Rossby number in the atmosphere is small. We will see in Section 9.3 that $R_o \simeq 10^{-3}$ for large-scale ocean circulation.

The smallness of R_o for large-scale motion in the free atmosphere and ocean[4] implies that the acceleration term in Eq.(6.43) dominates the Coriolis term, leaving

$$f\hat{\mathbf{z}}\times\mathbf{u} + \frac{1}{\rho}\nabla p = 0\ . \tag{7.2}$$

Equation (7.2) defines *geostrophic balance*, in which the pressure gradient is balanced by the Coriolis term. We expect this balance to be approximately satisfied for flows of small R_o. Another way of saying the same thing is

waves, the Rossby number and the Rossby radius of deformation, all ideas fundamental to the understanding of all planetary scale fluids.

[4]Near the equator, where $f \to 0$, the small Rossby number assumption breaks down, as will be seen, *e.g.*, in Section 12.2.2, below.

that, if we define the *geostrophic wind*, or *current*, to be the velocity $\mathbf{u}_g$ that *exactly* satisfies Eq.(7.2), then $\mathbf{u} \simeq \mathbf{u}_g$ in such flows. Since $\hat{\mathbf{z}} \times \hat{\mathbf{z}} \times \mathbf{u} = -\mathbf{u}$, (7.2) gives

$$\mathbf{u}_g = \frac{1}{f\rho}\hat{\mathbf{z}} \times \nabla p \ , \tag{7.3}$$

or, in component form in the local Cartesian geometry of Fig.6.19,

$$(u_g, v_g) = \left(-\frac{1}{f\rho}\frac{\partial p}{\partial y}, \frac{1}{f\rho}\frac{\partial p}{\partial x} \right) \ . \tag{7.4}$$

The geostrophic balance of forces described by (7.2) is illustrated in Fig.7.1. The pressure gradient force is, of course, directed away from the high pressure system on the left, and towards the low pressure system on the right. The balancing Coriolis forces must be as shown, directed in the opposite sense, and consequently the geostrophically balanced flow must be *normal* to the pressure gradient, *i.e.*, along the contours of constant pressure, as Eq.(7.3) makes explicit. For the northern hemisphere cases ($f > 0$) illustrated in Fig.7.1, the sense of the flow is clockwise around a high pressure system, and anticlockwise around a low. (The sense is opposite in the southern hemisphere.) The rule is summarized in Buys-Ballot's (the 19th century Dutch meteorologist) law:

> If you stand with you back to the wind in the northern hemisphere, low pressure is on your left

("left"→"right" in the southern hemisphere).

As Eq.(7.3) makes explicit, the geostrophic flow depends on the magnitude of the pressure gradient, and not just its direction. Consider Fig.7.2, on which the curved lines show two isobars of constant pressure p and $p+\delta p$, separated by the variable distance δs. From Eq.(7.3),

$$|\mathbf{u}_g| = \frac{1}{f\rho}\,|\nabla p| = \frac{1}{f\rho}\frac{\delta p}{\delta s} \ .$$

Since δp is constant along the flow, $|\mathbf{u}_g| \propto (\delta s)^{-1}$; the flow is strongest where the isobars are closest together. The geostrophic flow does not cross the pressure contours, and so the latter act like the banks of a river, causing the flow to speed up where the river is narrow and to slow down where it is wide. These characteristics explain, in large part, why the meteorologist is

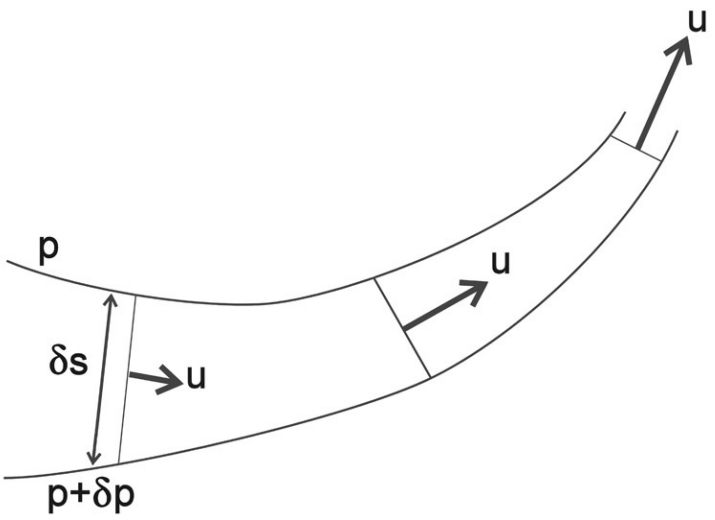

Figure 7.2: Schematic of two pressure contours (isobars) on a horizontal surface. The geostrophic flow, defined by Eq.(7.3), is directed along the isobars; its magnitude increases as the isobars become closer together.

traditionally preoccupied with pressure maps: the pressure field determines the winds.

Note that the vertical component of the geostrophic flow, as defined by Eq.(7.3), is zero. This cannot be deduced directly from Eq.(7.2), which involves the horizontal components of the flow. However, consider for a moment an incompressible fluid (in the laboratory or the ocean) for which we can neglect variations in ρ. Further, while f varies on the sphere, it is almost constant over scales of, say, 1000 km or less[5]. Then Eq.(7.4) gives

$$\frac{\partial u_g}{\partial x} + \frac{\partial v_g}{\partial y} = 0 \ . \tag{7.5}$$

Thus, the geostrophic flow is horizontally *non-divergent*. Comparison with the continuity Eq.(6.11) then tells us that $\partial w_g/\partial z = 0$; if $w_g = 0$ on, say, a flat bottom boundary, then it follows that $w_g = 0$ everywhere, and so the geostrophic flow is, indeed, horizontal.

[5]Variations of f do matter, however, for motions of planetary scale, as will be seen for example in Section 10.2.1.

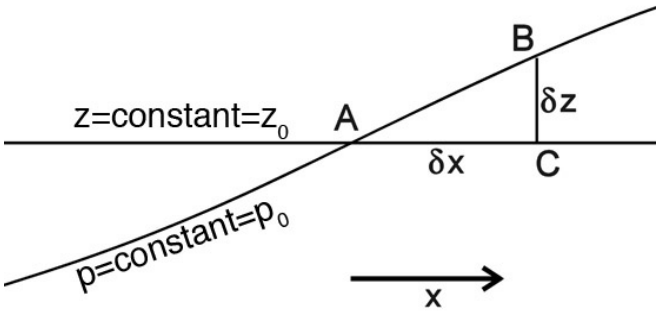

Figure 7.3: Schematic used in converting from pressure gradients on height surfaces to height gradients on pressure surfaces.

In a compressible fluid such as the atmosphere, density variations complicate matters. We therefore now consider the equations of geostrophic balance in pressure coordinates, in which case such complications do not arise.

7.1.1 The geostrophic wind in pressure coordinates

In order to apply the geostrophic equations to atmospheric observations and particularly to upper air analyses (see below), we need to express them in terms of height gradients on a pressure surface, rather than, as in Eq.(7.4), of pressure gradients at constant height.

Consider Fig.7.3. The figure depicts a surface of constant height z_0, and one of constant pressure p_0, which intersect at A, where of course pressure is $p_A = p_0$ and height is $z_A = z_0$. At constant height, the gradient of pressure in the x-direction is

$$\left(\frac{\partial p}{\partial x}\right)_z = \frac{p_C - p_0}{\delta x} \tag{7.6}$$

where δx is the (small) distance between C and A and subscript z means 'keep z constant'. Now, the gradient of height along the constant pressure surface is

$$\left(\frac{\partial z}{\partial x}\right)_p = \frac{z_B - z_0}{\delta x} \ .$$

subscript p means 'keep p constant'. Since $z_C = z_0$, and $p_B = p_0$, we can use

the hydrostatic balance equation Eq.(3.3) to write

$$\frac{p_C - p_0}{z_B - z_0} = \frac{p_C - p_B}{z_B - z_C} = -\frac{\partial p}{\partial z} = g\rho$$

and so $p_C - p_0 = g\rho\,(z_B - z_0)$.

Therefore from Eq.(7.6), and invoking a similar result in the y-direction, it follows that

$$\begin{aligned} \left(\frac{\partial p}{\partial x}\right)_z &= g\rho\left(\frac{\partial z}{\partial x}\right)_p ; \\ \left(\frac{\partial p}{\partial y}\right)_z &= g\rho\left(\frac{\partial z}{\partial y}\right)_p . \end{aligned}$$

In pressure coordinates Eq.(7.3) thus becomes:

$$\mathbf{u}_g = \frac{g}{f}\widehat{\mathbf{z}_p} \times \nabla_p z \ , \tag{7.7}$$

where $\widehat{\mathbf{z}_p}$ is the upward unit vector in pressure coordinates and ∇_p denotes the gradient operator in pressure coordinates. In component form it is,

$$(u_g, v_g) = \left(-\frac{g}{f}\frac{\partial z}{\partial y}, \frac{g}{f}\frac{\partial z}{\partial x}\right) \ . \tag{7.8}$$

The wonderful simplification of Eq.(7.8) relative to (7.4) is that ρ does not explicitly appear and therefore, in evaluation from observations, we need not be concerned about its variation. Just like p contours on surfaces of constant z, z contours on surfaces of constant p are streamlines of the geostrophic flow. The geostrophic wind is nondivergent in pressure coordinates if f is taken as constant:

$$\nabla_p \cdot \mathbf{u}_g = \frac{\partial u}{\partial x} + \frac{\partial v}{\partial y} = 0 \ . \tag{7.9}$$

Eq.(7.9) enables us to define a streamfunction:

$$u_g = -\frac{\partial \psi_g}{\partial y}; v_g = \frac{\partial \psi_g}{\partial x} \tag{7.10}$$

which, as can be verified by substitution, satisfies Eq.(7.8) for any $\psi_g = \psi_g(x, y, p, t)$. Comparing Eq.(7.10) with Eq.(7.8) we see that:

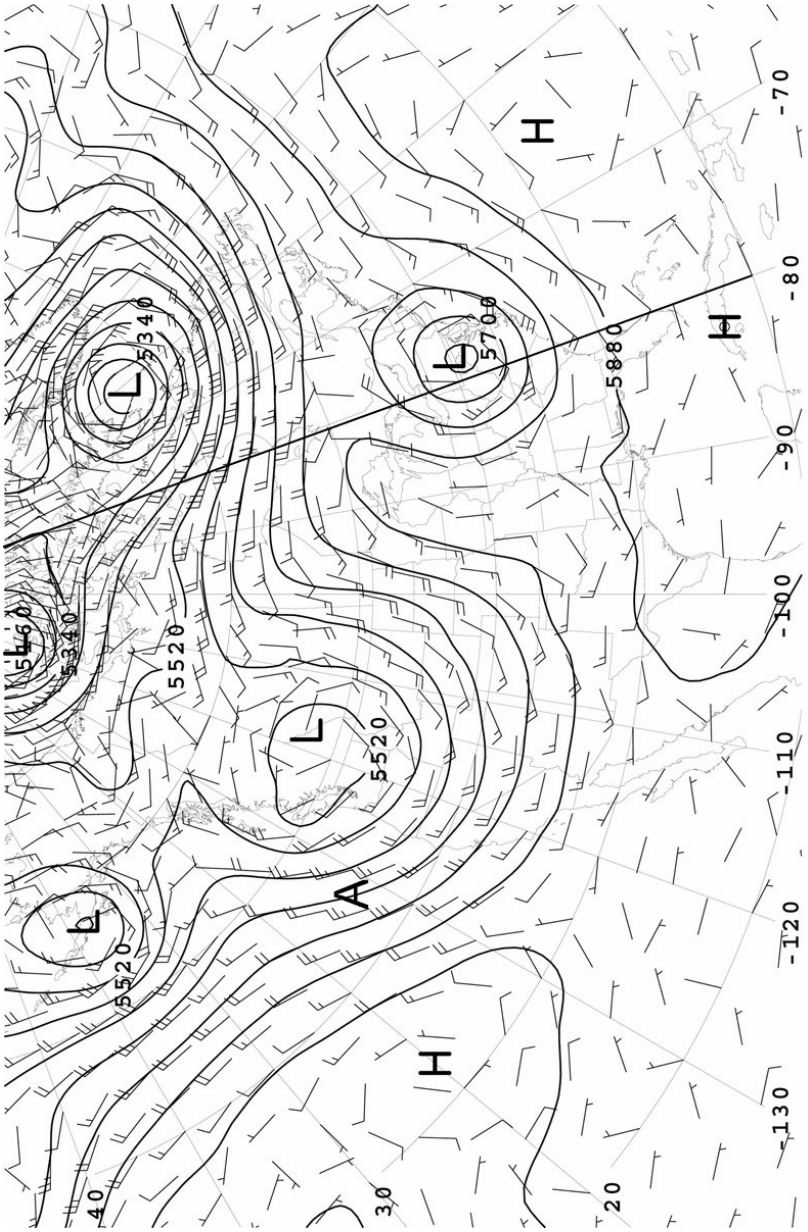

Figure 7.4: The 500 mbar wind and geopotential height field at 12GMT on June 21st, 2003. [Latitude and longitude (in degrees) are labelled by the numbers along the left and bottom edge of the plot.] The wind blows away from the quiver: one full quiver denotes a speed of $10\,\mathrm{m\,s^{-1}}$, one half-quiver a speed of $5\,\mathrm{m\,s^{-1}}$. The geopotential height is contoured every 60 m. Centers of high and low pressure are marked H and L. The position marked A is used as a check on geostrophic balance. The thick black line marks the position of the meridional section shown in Fig. 7.21 at 80°W extending from 20°N to 70°N. This section is also marked on Figs. 7.5 , 7.20 and 7.25.

$$\psi_g = \frac{g}{f} z. \tag{7.11}$$

Thus height contours are *streamlines of the geostrophic flow* on pressure surfaces: the geostrophic flow streams along z contours, as can be seen in Fig.7.4). This is in large part why the meteorologist is preoccupied with the field of $z(p)$: when interpreted in terms of the geostrophic relation, they reveal the winds.

What does Eq.(7.8) imply about the magnitude of the wind? In Fig.5.13 we saw that the 500 mbar pressure surface slopes down by a height $\Delta z = 800\,\mathrm{m}$ over a meridional distance $L = 5000\,\mathrm{km}$; then geostrophic balance implies a wind of strength $u = \frac{g}{f}\frac{\Delta z}{L} = \frac{9.81}{10^{-4}}\frac{800}{5\times10^6} \approx 15\,\mathrm{m\,s^{-1}}$.

Thus Coriolis forces acting on a zonal wind of speed $\sim 15\,\mathrm{m\,s^{-1}}$, are of sufficient magnitude to balance the poleward pressure gradient force associated with the pole-equator temperature gradient. This is just what is observed; see the strength of the mid-level flow shown in Fig.5.20. Geostrophic balance thus 'connects' Figs.5.13 and 5.20 together.

Let us now look at some synoptic charts such as those shown in Fig.5.22 and 7.4, to see geostrophic balance in action.

7.1.2 Highs and Lows; synoptic charts

Fig.7.4 shows the height of the 500mb surface (contoured every 60 m) plotted with the observed wind vector (one full quiver represents a wind speed of 10 $\mathrm{m\,s^{-1}}$) at an instant in time: 12GMT on June 21st, 2003, to be exact, the same time as the hemispheric map shown in Fig.5.22. Note how the wind blows along the height contours and is strongest the closer the contours are together, just as saw see in Fig.7.1. At this level, away from frictional effects at the ground, the wind is close to geostrophic.

Consider, for example, the point marked by the left 'foot' of the 'A' shown in Fig.7.4, at 43°N, 133°W. The wind is blowing along the height contours to the SSE at a speed of $25\,\mathrm{m\,s^{-1}}$. We estimate that the 500 mbar height surface slopes down at a rate of 60 m in 250 km here (noting that 1° of latitude is equivalent to a distance of 111 km and that the contour interval is 60 m). The geostrophic relation, Eq.(7.7), then implies a wind of speed $\frac{g}{f}\frac{\Delta z}{L} = \frac{9.81}{9.7\times10^{-5}}\frac{60}{2.5\times10^5} = 24\,\mathrm{m\,s^{-1}}$, close to that observed. Indeed the wind at upper levels in the atmosphere is very close to geostrophic balance.

In Fig.7.5 we plot the R_o (calculated as $|\mathbf{u}\cdot\nabla\mathbf{u}| \,/\, |f\mathbf{u}|$) for the synoptic pattern shown in Fig.7.4. It is about 0.1 over most of the region and so the flow is to a good approximation in geostrophic balance. However R_o can approach unity in intense low pressure systems where the flow is strong and the flow curvature large, such as in the low centered over 80°W, 40°N. Here the Coriolis and advection terms are of comparable magnitude to one another and there is a 3-way balance between Coriolis, inertial and pressure gradient forces. Such a balance is known as 'gradient wind balance' — see Section 7.1.3 below.

7.1.3 Balanced flow in the radial-inflow experiment

At this point it is useful to return to the radial inflow experiment — GFD Lab III, described in Section 6.6.1 — and compute the Rossby number assuming that axial angular momentum of fluid parcels is conserved as they spiral into the drain hole (see Fig.6.6). The Rossby number implied by Eq.(6.23) is given by:

$$R_o = \frac{v_\theta}{2\Omega r} = \frac{1}{2}\left(\frac{r_1^2}{r^2} - 1\right) \tag{7.12}$$

where r_1 is the outer radius of the tank. It is plotted as a function of $\frac{r}{r_1}$ in Fig.7.6(right).

The observed R_o, based on tracking particles floating on the surface of the fluid (see Fig.6.6) together with the theoretical prediction, (7.12), are plotted in Fig.7.6. We see broad agreement, but the observations depart from the theoretical curve at small r and high R_o, due, perhaps, to the difficulty of tracking the particles in the high speed core of the vortex (note the blurring of the particles at small radius evident in Fig.6.6).

According to Eq.(7.12) and Fig.7.6, $R_o = 0$ at $r = r_1$, $R_o = 1$ at a radius $\frac{r_1}{\sqrt{3}} = 0.58 r_1$, and rapidly increases as r decreases further. Thus the azimuthal flow is geostrophically balanced in the outer regions (small R_o) with the radial pressure gradient force balancing the Coriolis force in Eq.(6.21). In the inner regions (high R_o) the $\frac{v_\theta^2}{r}$ term in Eq.(6.21) balances the radial pressure gradient — this is known as 'cyclostrophic balance'. In the middle region (where $R_o \sim 1$) all three terms in Eq.(6.21) play a role; this is known as 'gradient wind balance' of which geostrophic and cyclostrophic balance are limiting cases. As mentioned earlier, gradient wind balance can

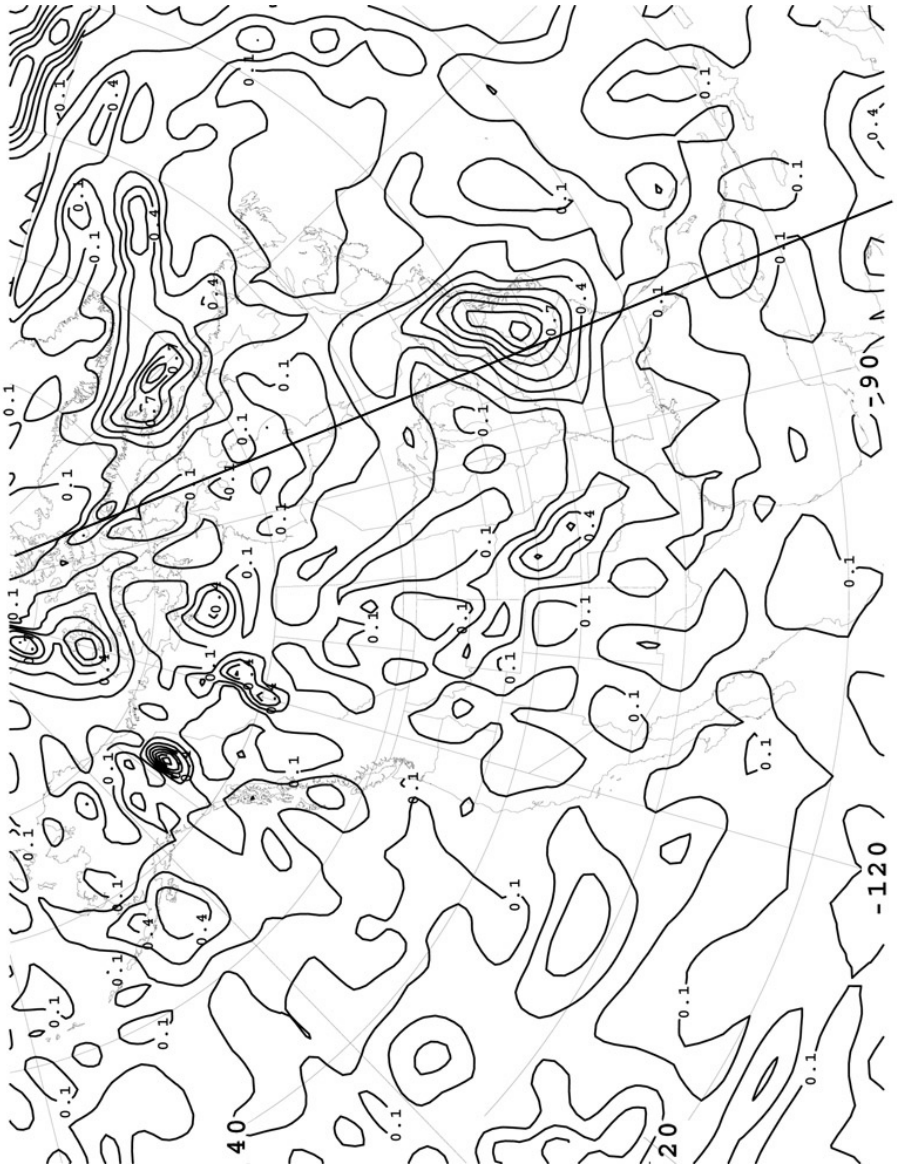

Figure 7.5: The Rossby number for the 500 mbar flow at 12GMT on June 21st, 2003, the same time as Fig.7.4. The contour interval is 0.1. Note that $R_o \sim 0.1$ over most of the region but can approach 1 in strong cyclones, such as the low centered over 80°W, 40°N.

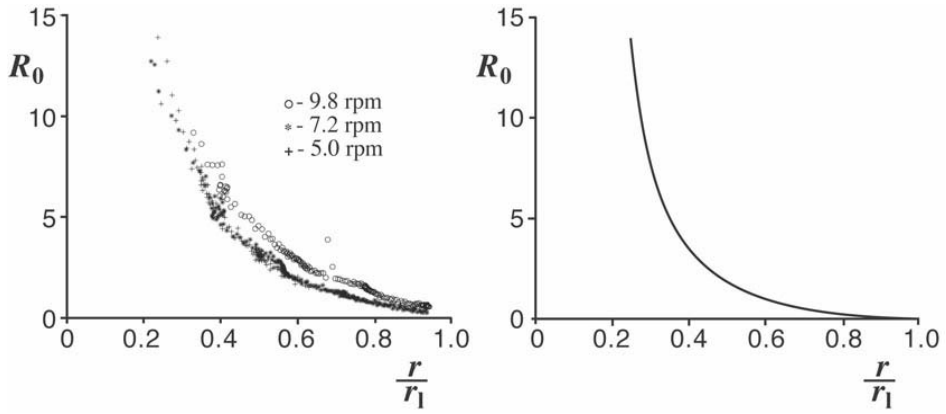

Figure 7.6: Left: the R_o number plotted as a function of non-dimensional radius ($\frac{r}{r_1}$) computed by tracking particles in three radial inflow experiments (each at a different rotation rate — quoted here in revolutions per minute (rpm)). Right: theoretical prediction based on Eq.(7.12).

be seen in the synoptic chart shown in Fig.7.4, in the low pressure regions where $R_o \sim 1$ (Fig.7.5).

7.2 The Taylor-Proudman Theorem

A remarkable property of geostrophic motion is that if the fluid is homogeneous (ρ uniform) then, as we shall see, the geostrophic flow is two dimensional and does not vary in the direction of the rotation vector, $\mathbf{\Omega}$. Known as the Taylor-Proudman theorem, we discuss this statement here and make much subsequent use of it — particularly in Chapters 10 and 11 — to discuss the constraints of rotation on the motion of the atmosphere and ocean.

For the simplest derivation of the theorem let us begin with the geostrophic relation written out in component form, Eq.(7.4). If ρ and f are constant, then taking the vertical derivative of the geostrophic flow components and using hydrostatic balance, we see that $\left(\frac{\partial u_g}{\partial z}, \frac{\partial v_g}{\partial z}\right) = 0$: i.e. the geostrophic flow does not vary in the direction of $f\widehat{\mathbf{z}}$.

A slightly more general statement of this result can be obtained if we go right back to the pristine form of the momentum equation (6.29) in rotating coordinate. If the flow is sufficiently slow and steady ($R_o << 1$) and $\mathcal{F}$ is

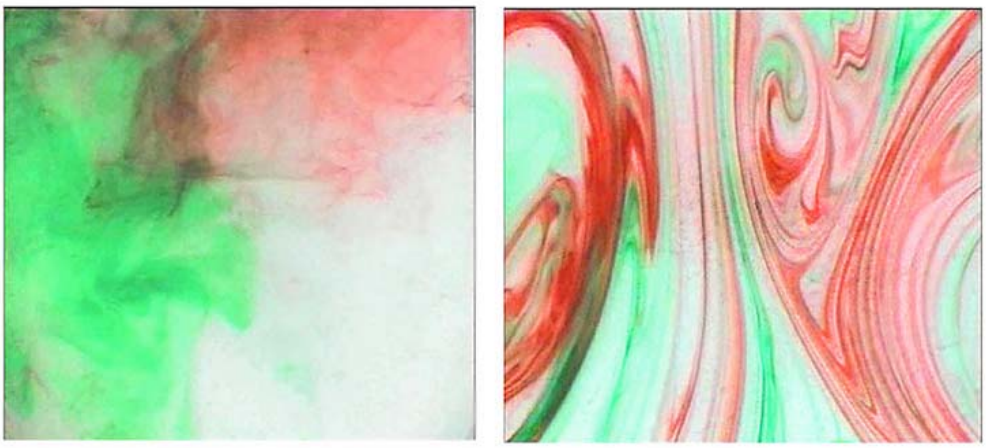

Figure 7.7: Dye distributions from GFD Lab 0: on the left we see a pattern from dyes (colored red and green) stirred into a non-rotating fluid in which the turbulence is three-dimensional; on the right we see dye patterns obtained in a rotating fluid in which the turbulence occurs in planes perpendicular to the rotation axis and is thus two-dimensional.

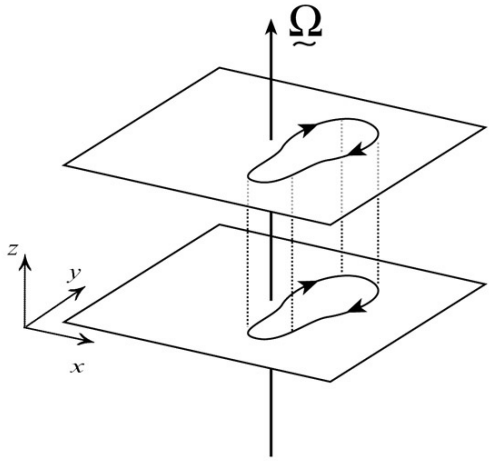

Figure 7.8: The Taylor-Proudman theorem, Eq.(7.14), states that slow, steady, frictionless flow of a barotropic, incompressible fluid is 2-dimensional and does not vary in the direction of the rotation vector Ω.

negligible, it reduces to:

$$2\boldsymbol{\Omega} \times \mathbf{u} \; + \; \frac{1}{\rho}\nabla p \; + \; \nabla\phi = 0 \tag{7.13}$$

The horizontal component of Eq.(7.13) yields geostrophic balance — Eq.(7.2) or Eq.(7.4) in component form — where now $\widehat{\mathbf{z}}$ is imagined to point in the direction of $\boldsymbol{\Omega}$ — see Fig.7.8. The vertical component of Eq.(7.13) yields hydrostatic balance, Eq.(3.3). Taking the curl ($\nabla\times$) of Eq.(7.13), we find that if the fluid is *barotropic* (i.e. one in which $\rho = \rho(p)$) then:[6]

$$(\; \boldsymbol{\Omega}.\nabla)\, \mathbf{u} = 0 \tag{7.14}$$

or (since $\boldsymbol{\Omega}.\nabla$ is the gradient operator in the direction of $\boldsymbol{\Omega}$ i.e. $\widehat{\mathbf{z}}$)

$$\frac{\partial \mathbf{u}}{\partial z} = 0. \tag{7.15}$$

Equation (7.14) is known as the Taylor-Proudman theorem (or T-P for short). T-P says that under the stated conditions — slow, steady, frictionless flow of a barotropic fluid — the velocity $\mathbf{u}$, both horizontal and vertical components, cannot vary in the direction of the rotation vector $\boldsymbol{\Omega}$. In other words the flow is two–dimensional, as sketched in Fig.7.8. Thus, vertical columns of fluid remain vertical — they cannot be tilted over or stretched: we say that the fluid is made 'stiff' in the direction of $\boldsymbol{\Omega}$. The columns are called 'Taylor Columns' after G.I. Taylor who first demonstrated them experimentally[7].

[6] Using vector identities 2. and 6. of Appendix 13.2, setting $\mathbf{a} \longrightarrow \boldsymbol{\Omega}$ and $\mathbf{b} \longrightarrow \mathbf{u}$, remembering that $\nabla \cdot \mathbf{u} = 0$ and $\nabla \times \nabla(\text{scalar}) = 0$.

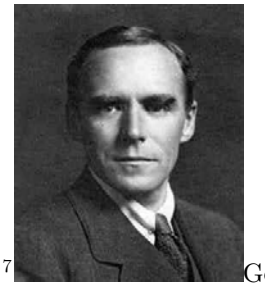

[7] Geoffrey Ingram Taylor (1886–1975). British scientist who made fundamental and long-lasting contributions to a wide range of scientific problems, especially theoretical and experimental investigations of fluid dynamics. The result Eq.(7.14) was first demonstrated by Joseph Proudman in 1915 but is now called the Taylor–Proudman theorem. Taylor's name got attached because he demonstrated the theorem

Rigidity, imparted to the fluid by rotation, is at the heart of the glorious dye patterns seen in experiment GFD Lab 0. On the right of Fig.7.7, the rotating fluid, brought in to gentle motion by stirring, is constrained to move in two-dimensions. Rich dye patterns emerge in planes perpendicular to $\mathbf{\Omega}$ but with strong vertical coherence between the levels: flow at one horizontal level moves in lockstep with the flow at another level. In contrast, a stirred non-rotating fluid mixes in three dimensions and has an entirely different character with no vertical coherence; see the left frame of Fig.7.7.

Taylor columns can readily be observed in the laboratory in a more controlled setting, as we now go on to describe.

7.2.1 GFD Lab VII: 'Taylor columns'

Suppose a homogeneous rotating fluid moves in a layer of variable depth, as sketched in Fig.7.9. This can easily be arranged in the laboratory by placing an obstacle (such as a bump made of a plastic pillbox) in the bottom of a tank of water rotating on a turntable and observing the flow of water past the obstacle, as depicted in Fig.7.9. The T-P theorem demands that vertical columns of fluid move along contours of constant fluid depth because they cannot be stretched.

At levels below the top of the obstacle, the flow must of course go around it. But Eq.(7.15) says that the flow must be the same at all z: so, at all heights, the flow must be deflected as if the bump on the boundary extended all the way through the fluid! We can demonstrate this behavior in the laboratory, using the apparatus sketched in Fig.7.10 and described in the legend, by inducing flow past a submerged object.

We see the flow (marked by paper dots floating on the free surface) being diverted around the obstacles in a vertically coherent way (as shown in the photograph of Fig.7.11) as if the obstacle extended all the way through the water, thus creating stagnant "Taylor columns" above the obstacle.

---

experimentally — see GFD Lab VII. In a paper published in 1921, he reported slowly dragging a cylinder through a rotating flow. The solid object all but immobilized an entire column of fluid parallel to the rotation axis.

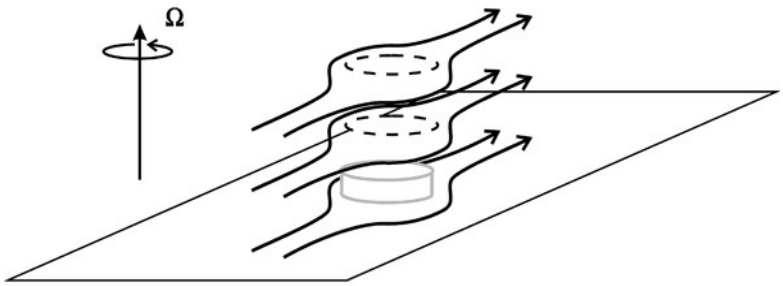

Figure 7.9: The T-P theorem demands that vertical columns of fluid move along contours of constant fluid depth because, from Eq.(7.14), $\partial w/\partial z = 0$ and therefore they cannot be stretched. Thus fluid columns act as if they were rigid columns and move along contours of constant fluid depth. Horizontal flow is thus deflected as if the obstable extended through the whole depth of the fluid.

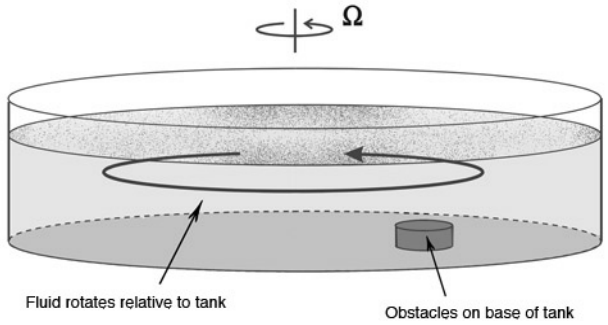

Figure 7.10: We place a cylindrical tank of water on a table turning at about 5 rpm. An obstacle is placed on the base of the tank whose height is a small fraction of the fluid depth; the water is left until it comes into solid body rotation. We now make a very small reduction in Ω (by 0.1 rpm or less). Until a new equilibrium is established (the "spin-down" process takes several minutes, depending on rotation rate and water depth), horizontal flow will be induced relative to the obstacle. Dots on the surface, used to visualize the flow — see Fig.7.11 — reveal that the flow moves around the obstacle as if the obstacle extended through the whole depth of the fluid.

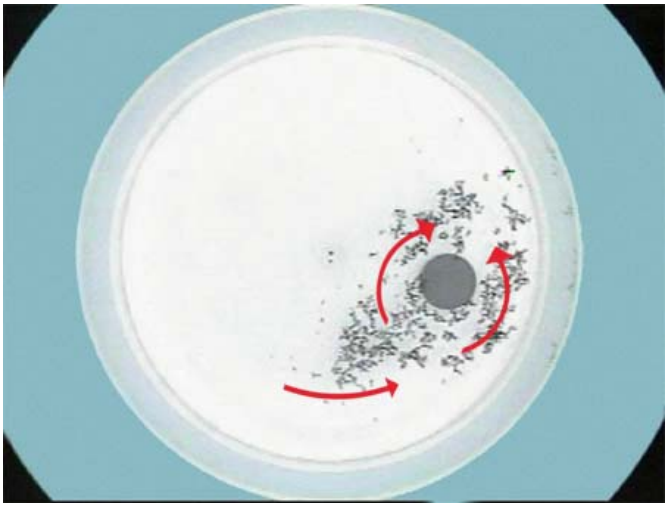

Figure 7.11: Paper dots on the surface of the fluid shown in the experiment described in Fig. 7.10. The dots move around, but not over, a submerged obstacle, in experimental confirmation of the schematic drawn in Fig.7.9.

7.3 The thermal wind equation

We saw in Section 5.2 that isobaric surfaces slope down from equator to pole. Moreover, these slopes increase with height, as can be seen, for example, in Fig.5.13 and the schematic diagram, Fig.5.14. Thus according to the geostrophic relation, Eq.(7.8), the geostrophic flow will increase with height, as indeed is observed in Fig.5.20. According to T-P, however, $\frac{\partial \mathbf{u}_g}{\partial z} = 0$. What's going on?

The Taylor-Proudman theorem pertains to a slow, steady, frictionless, barotropic fluid in which $\rho = \rho(p)$. But in the atmosphere and ocean, density does vary on pressure surfaces and so T-P does not strictly apply and must be modified to allow for density variations.

Let us again consider the water in our rotating tank but now suppose that the density of the water varies thus:

$$\rho = \rho_{ref} + \sigma \text{ and } \frac{\sigma}{\rho_{ref}} << 1$$

where ρ_{ref} is a constant reference density, and σ — called the density *anomaly*

— is the variation of the density about this reference.[8]

Now take $\partial/\partial z$ of Eq.(7.4) (replacing ρ by ρ_{ref} where it appears in the denominator) we obtain, making use of the hydrostatic relation Eq.(3.3):

$$\left(\frac{\partial u_g}{\partial z}, \frac{\partial v_g}{\partial z}\right) = \frac{g}{f\rho_{ref}}\left(\frac{\partial \sigma}{\partial y}, -\frac{\partial \sigma}{\partial x}\right) \tag{7.16}$$

or, in vector notation (see Appendix 13.2, VI)

$$\frac{\partial \mathbf{u}_g}{\partial z} = -\frac{g}{f\rho_{ref}}\widehat{\mathbf{z}} \times \boldsymbol{\nabla}\sigma \ . \tag{7.17}$$

So if ρ varies in the horizontal then the geostrophic current will vary in the vertical. To express things in terms of temperature, and hence derive a connection (called the *thermal wind* equation) between the current and the thermal field, we can use our simplified equation of state for water, Eq.(4.4), which assumes that the density of water depends on temperature T in a linear fashion. Then Eq.(7.17) can be written:

$$\frac{\partial \mathbf{u}_g}{\partial z} = \frac{\alpha g}{f}\widehat{\mathbf{z}} \times \boldsymbol{\nabla} T \tag{7.18}$$

where α is the thermal expansion coefficient. This is a simple form of the *thermal wind* relation connecting the vertical shear of the geostrophic current to horizontal temperature gradients. It tells us nothing more than the hydrostatic and geostrophic balances Eq.(3.3) and Eq.(7.4), but it expresses these balances in a different way.

We see that there is an exactly analogous relationship between $\frac{\partial \mathbf{u}_g}{\partial z}$ and T as between $\mathbf{u}_g$ and p: compare Eqs.(7.18) and (7.3). So if we have horizontal gradients of temperature then the geostrophic flow will vary with height. The westerly winds increase with height because, through the thermal wind relation, they are associated with the poleward decrease in temperature. We now go on to study the thermal wind in a laboratory setting in which we represent the cold pole by placing an ice bucket in the centre of a rotating tank of water.

[8] Typically the density of the water in the rotating tank experiments, and indeed in the ocean too (see Section 9.1.3) varies by only a few % about its reference value. Thus $\frac{\sigma}{\rho_{ref}}$ is indeed very small.

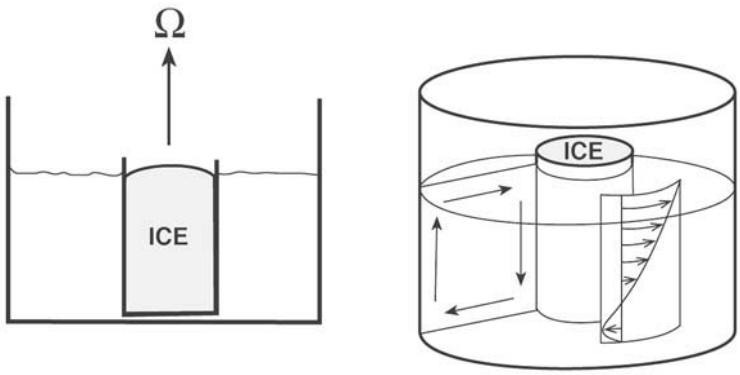

Figure 7.12: To study the thermal wind relation, we fill a cylindrical tank with water to a depth of 10 cm, and rotate it very slowly (1 rpm or less). The can of ice in the middle induces a radial temperature gradient. A thermal wind shear develops in balance with it, which can be visualized with dye, as sketched on the right. The experiment is left for 5 minutes or so for the circulation to develop. The radial temperature gradient is monitored with thermometers and the currents measured by tracking paper dots floating on the surface.

7.3.1 GFD Lab VIII: The thermal wind relation

It is straightforward to obtain a steady, axially-symmetric circulation driven by radial temperature gradients in our laboratory tank, which provides an ideal opportunity to study the thermal wind relation and the way in which vertical shears of geostrophic currents are generated by horizontal density gradients.

The apparatus is sketched in Fig.7.12 and can be seen in Fig.7.13. The cylindrical tank, at the center of which is an ice bucket, is rotated very slowly in an anticlockwise sense. The cold sides of the can cool the water adjacent to it and induce a radial temperature gradient. Paper dots sprinkled over the surface move in the same sense as, but more swiftly than, the rotating table — we have generated westerly (to the east) currents! We inject some dye; the dye streaks do not remain vertical but tilt over in an azimuthal direction, carried along by currents which increase in strength with height and are directed in the same sense as the rotating table (see the photograph in Fig.7.13 and the schematic Fig.7.14). The Taylor Columns have been tilted over by the westerly currents.

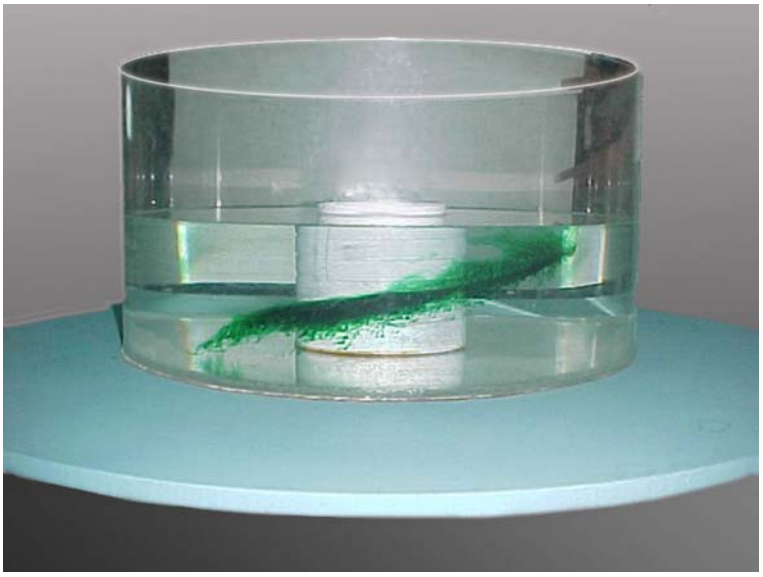

Figure 7.13: Dye streaks being tilted over in to a cork-screw pattern by an azimuthal current in thermal wind balance with a radial temperature gradient maintained by the ice bucket at the center.

For our incompressible fluid in cylindrical geometry (see Appendix 13.2.3), the azimuthal component of the thermal wind relation, Eq.(7.18), is:

$$\frac{\partial v_\theta}{\partial z} = \frac{\alpha g}{2\Omega}\frac{\partial T}{\partial r} \ ,$$

where v_θ is the azimuthal current (cf. Fig.6.8) and f has been replaced by 2Ω. Since T increases moving outwards from the cold center ($\partial T/\partial r > 0$) then, for positive Ω, $\partial v_\theta/\partial z > 0$. Since v_θ is constrained by friction to be weak at the bottom of the tank, we therefore expect to see $v_\theta > 0$ at the top, with the strongest flow at the radius of maximum density gradient. Dye streaks visible in Fig.7.13 clearly show the thermal wind shear, especially near the cold can where the density gradient is strong.

We note the temperature difference, ΔT, between the inner and outer walls a distance L apart (of order 1 °C per 10 cm), and the speed of the paper dots at the surface relative to the tank (typically 1 cm s^{-1}). The tank is turning at 1 rpm, and the depth of water is $H \sim 10$ cm. From the above thermal wind equation we estimate that:

$$\mathbf{u}_g \sim \frac{\alpha g}{2\Omega}\frac{\mathbf{\Delta}T}{L}H \sim 1\,\mathrm{cm\,s^{-1}}$$

for $\alpha = 2 \times 10^{-4}$ K^{-1}, roughly as we observe.

This experiment is discussed further in Section 8.2.1 as a simple analogue of the tropical Hadley circulation of the atmosphere.

7.3.2 The thermal wind equation and the Taylor-Proudman Theorem

The connection between the T-P theorem and the thermal wind equation can be better understood by noting that Eqs.(7.17) and (7.18) are simplified forms of a more general statement of the thermal wind equation which we now derive.

Taking $\nabla\times$[Eq.(7.13)], but now relaxing the assumption of a barotropic fluid, we obtain [noting that the term of the left of Eq.(7.13) transforms as in the derivation of Eq.(7.14) and that $\nabla \times \left(\frac{1}{\rho}\nabla p\right) = -\frac{1}{\rho^2}\nabla\rho \times \nabla p = \frac{1}{\rho^2}\nabla p \times \nabla\rho$]:

$$(2\mathbf{\Omega}\cdot\nabla)\,\mathbf{u} = \frac{1}{\rho}\nabla p \times \frac{1}{\rho}\nabla\rho \tag{7.19}$$

which is a more general statement of the 'thermal wind' relation. In the case of constant ρ, or, more precisely, in a barotropic fluid where $\rho = \rho(p)$ and so $\nabla\rho$ is parallel to ∇p, Eq.(7.19) reduces to (7.14). But now we are dealing with a baroclinic fluid in which density depends on temperature [see Eq.(4.4)] and so ρ surfaces and p surfaces are no longer coincident. Thus the term on the right of Eq.(7.19) — known as the baroclinic term — does not now vanish. It can be simplified by noting that, to a very good approximation, the fluid is in hydrostatic balance: $\frac{1}{\rho}\nabla p + g\widehat{\mathbf{z}} = \mathbf{0}$ allowing it to be written:

$$(2\mathbf{\Omega}\cdot\nabla)\,\mathbf{u} = 2\Omega\frac{\partial\mathbf{u}}{\partial z} = -\frac{g}{\rho}\widehat{\mathbf{z}}\times\nabla\rho. \tag{7.20}$$

When written in component form, Eq.(7.20) becomes Eq.(7.16) if $2\mathbf{\Omega} \longrightarrow f\widehat{\mathbf{z}}$ and $\rho \longrightarrow \rho_{ref} + \sigma$.

The physical interpretation of the right hand side of Eqs.(7.16) and (7.20) can now be better appreciated: it is the action of gravity on horizontal density gradients trying to return surfaces of constant density to the horizontal, the

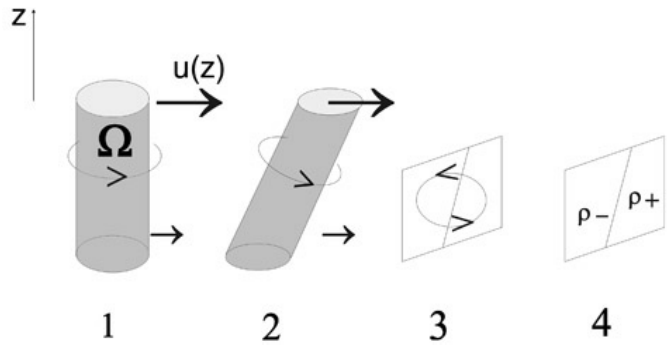

Figure 7.14: A schematic showing the physical content of the thermal wind equation written in the form Eq.(7.20): spin associated with the rotation vector $2\boldsymbol{\Omega}$ — [1] — is tilted over by the vertical shear (du/dz) [2]. Circulation in the transverse plane develops — [3] — creating horizontal density gradients from the stable vertical gradients. Gravity acting on the sloping density surfaces balances the overturning torque associated with the tilted Taylor Columns [4].

natural tendency of a fluid under gravity to find its own level. But on the large-scale this tendency is counter-balanced by the rigidity of the Taylor columns, represented by the term on the left of Eq.(7.20). How this works is sketched in Fig.7.14. The spin associated with the rotation vector $2\boldsymbol{\Omega}$ — [1] — is tilted over by the vertical shear (du/dz) of the current as time progresses [2]. Circulation in the transverse plane develops — [3] — and converts vertical stratification in to horizontal density gradients. If the environment is stably stratified, then the action of gravity acting on the sloping density surfaces is in the correct sense to balance the overturning torque associated with the tilted Taylor Columns [4]. This is the torque balance at the heart of the thermal wind relation.

We can now appreciate how it is that gravity fails to return inclined temperature surfaces, such as those shown in Fig.5.7, to the horizontal. It is prevented from doing so by the Earth's rotation.

7.3.3 GFD Lab IX: cylinder 'collapse' under gravity and rotation

A vivid illustration of the role that rotation plays in counteracting the action of gravity on sloping density surfaces can be carried out by creating a density front in a rotating fluid in the laboratory, as shown in Fig.7.15 and described in the legend. An initially vertical column of dense salty water is allowed to slump under gravity but is 'held up' by rotation forming a cone whose sides have a distinct slope. The photographs in Fig.7.16 show the development of a cone. The cone acquires a definite sense of rotation, swirling in the same sense of rotation as the table. We measure typical speeds through the use of paper dots, measure the density of the dyed water and the slope of the side of the cone (the front), and interpret them in terms of the following theory.

Theory following Margules

A simple and instructive model of a front can be constructed as follows. Suppose that the density is ρ_1 on one side of the front and changes discontinuously to ρ_2 on the other, with $\rho_1 > \rho_2$ as sketched in Fig.7.17. Let y be a horizontal axis normal to the discontinuity and let γ be the angle that the surface of discontinuity makes with the horizontal. Since the pressure must be the same on both sides of the front then the pressure change computed along paths [1] and [2] in Fig.7.17 must be the same since they begin and end at common points in the fluid:

$$\left(\frac{\partial p}{\partial z}\delta z + \frac{\partial p}{\partial y}\delta y\right)_{\text{path 2}} = \left(\frac{\partial p}{\partial y}\delta y + \frac{\partial p}{\partial z}\delta z\right)_{\text{path 1}}$$

for small δy, δz. Hence, using hydrostatic balance to express $\frac{\partial p}{\partial z}$ in terms of ρg on both sides of the front, we find:

$$\tan\gamma = \frac{dz}{dy} = \frac{\frac{\partial p_1}{\partial y} - \frac{\partial p_2}{\partial y}}{g\left(\rho_{_1} - \rho_{_2}\right)}.$$

Using the geostrophic approximation to the current, Eq.(7.4), to relate the pressure gradient terms to flow speeds, we arrive at the following form of the thermal wind equation (which should be compared to Eq.(7.16)):

$$\left(u_{_2} - u_{_1}\right) = \frac{g'\tan\gamma}{2\Omega} \tag{7.21}$$

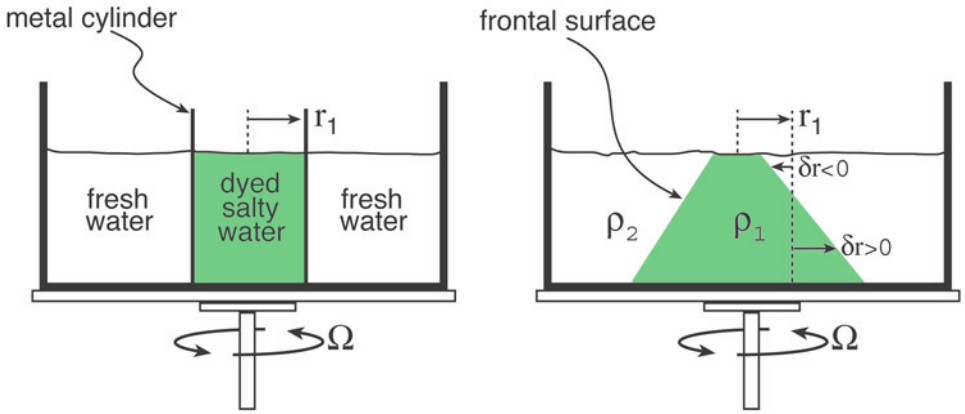

Figure 7.15: We place a large tank on our rotating table, fill it with water to a depth of 10 cm or so and place in the center of it a hollow metal cylinder of radius $r_1 = 6$ cm which protrudes slightly above the surface. The table is set into rapid rotation at a speed of 10 rpm and allowed to settle down for 10 minutes or so. Whilst the table is rotating the water within the cylinder is carefully and slowly replaced by dyed, salty (and hence dense) water delivered from a large syringe. When the hollow cylinder is full of colored saline water, it is rapidly removed in a manner which causes the least disturbance possible — practice is necessary! The subsequent evolution of the dense column is charted in Fig.7.16. The final state is sketched on the right: the cylinder has collapsed into a cone whose surface is displaced a distance δr relative to that of the original upright cylinder.

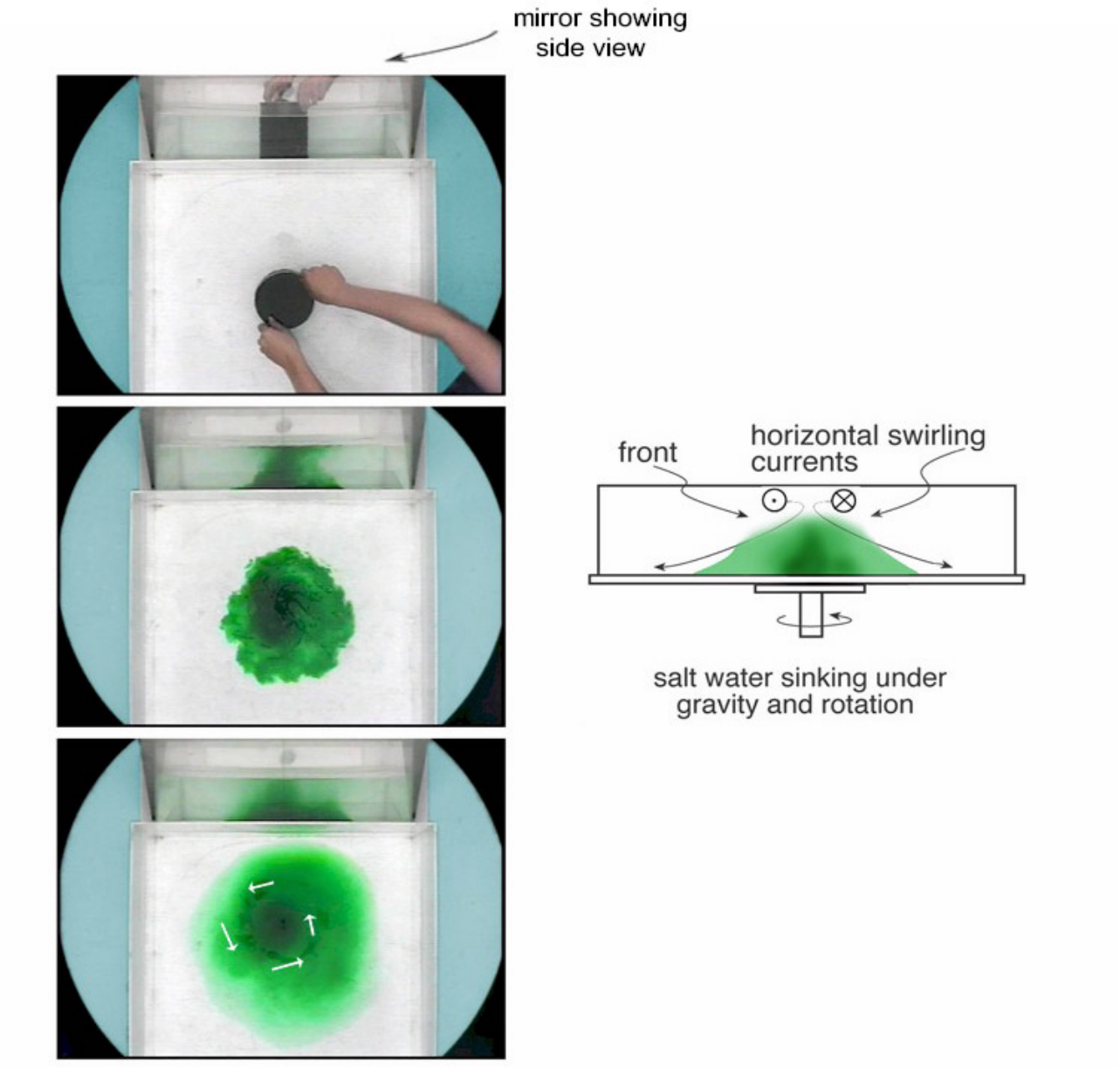

Figure 7.16: (left) Series of pictures charting the creation of a dome of salty (and hence dense) dyed fluid collapsing under gravity and rotation. The fluid depth is some 10 cm. The white arrows indicate the sense of rotation of the dome. At the top of the figure we show a view through the side of the tank facilitated by a sloping mirror. (right) A schematic diagram of the dome showing its sense of circulation.

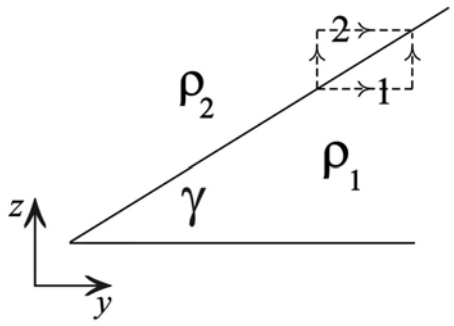

Figure 7.17: Geometry of the front separating fluid of differing densities used in the derivation of Margules relation, Eq.(7.21).

where u is the component of the current parallel to the front and $g' = g\frac{\Delta\rho}{\rho_1}$ is the 'reduced gravity' with $\Delta\rho = \rho_1 - \rho_2$ (cf. parcel 'buoyancy', defined in Eq.(4.3) of Section 4.2) . Eq.(7.21) is known as 'Margules relation' — a formula derived in 1903 by the Austrian meteorologist Max Margules, to explain the slope of boundaries in atmospheric fronts. Here it relates the swirl speed of the cone to g', γ, and Ω.

In the experiment we typically observe a slump angle γ of perhaps 30° for $\Omega \sim 1\,\mathrm{s}^{-1}$ (corresponding to a rotation rate of 10rpm) and a $g' \sim 0.2\,\mathrm{m\,s}^{-2}$ (corresponding to a $\frac{\Delta\rho}{\rho}$ of some 2%). Eq.(7.21) then predicts a swirl speed of about $6\,\mathrm{cm\,s}^{-1}$, broadly in accord with what is observed in the high-speed core of the swirling cone.

Finally, to make the connection of the experiment with the atmosphere more explicit, we show in Fig.7.18 the dome of cold air that exists over the north pole and the strong upper-level wind associated with it. The horizontal temperature gradients and vertical wind shear are in thermal wind balance on the planetary scale.

7.3.4 Mutual adjustment of velocity and pressure

The cylinder collapse experiment encourages us to wonder about the adjustment between the velocity field and the pressure field. Initially (left frame of Fig.7.15) the cylinder is not in geostrophic balance. The 'end state', sketched in the right frame and being approached in Fig.7.16(bottom) and Fig.7.18, is in 'balance' and well described by Margules formula, Eq.(7.21). How far does

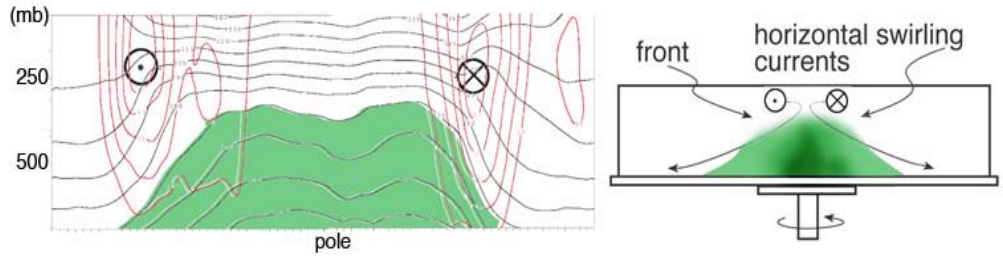

Figure 7.18: The dome of cold air that exists over the north pole shown in the instantaneous slice across the pole on the left (shaded green) is associated with strong upper-level winds marked $\otimes$ and $\odot$, and contoured in red. On the right we show a schematic diagram of the column of salty water studied in GFD Lab IX (cf. Figs.7.15 and 7.16. The column is prevented from slumping all the way to the bottom by the rotation of the tank. Differences in Coriolis forces acting on the spinning column provide a 'torque' which balances that of gravity acting on salty fluid trying to pull it down.

the cylinder have to slump sideways before the velocity field and the pressure field come in to this balanced state? This problem was of great interest to Rossby and is known as the 'Rossby adjustment problem'. The detailed answer is in general rather complicated but we can arrive at a qualitative estimate rather directly, as follows.

Let us suppose that the collapse of the column occurs conserving angular momentum so that $\Omega r^2 + ur =$ constant, where r is the distance from the center of the cone and u is the velocity at its edge. If r_1 is the initial radius of a stationary ring of salty fluid (on the left of Fig.7.15) then it will have an azimuthal speed given by:

$$u = -2\Omega\delta r \tag{7.22}$$

if it changes its radius by an amount δr (assumed small) as marked on the right of Fig.7.15. In the upper part of the water column, $\delta r < 0$ and the ring will acquire a cyclonic spin; below, $\delta r > 0$ and the ring will spin anticyclonically.[9] This slumping will proceed until the resulting vertical shear is enough

[9]In practice, friction caused by the cone of fluid rubbing over the bottom brings currents there toward zero. The thermal wind shear remains, however, with cyclonic flow increasing all the way up to the surface.

to satisfy Eq.(7.21). Assuming that $\tan\gamma \sim \frac{H}{|\delta r|}$ where H is the depth of the water column, combining Eqs.(7.22) and (7.21) we see that this will occur at a value of $\delta r \sim L_\rho = \frac{\sqrt{g'H}}{2\Omega}$. By noting that[10] $g'H \approx N^2H^2$, L_ρ can be expressed in terms of the buoyancy frequency N of a continuously stratified fluid thus:

$$L_\rho = \frac{\sqrt{g'H}}{2\Omega} = \frac{NH}{2\Omega} \tag{7.23}$$

where now H is interpreted as the vertical scale of the motion. The horizontal length scale Eq.(7.23) is known as the 'Rossby radius of deformation'. It is the scale at which the effects of rotation become comparable with those of stratification. More detailed analysis shows that on scales smaller than L_ρ the pressure adjusts to the velocity field whereas on scales much greater than L_ρ the reverse is true and the velocity adjusts to the pressure.

For the values of g' and Ω appropriate to our cylinder collapse experiment described above, $L_\rho \sim 7\,\text{cm}$ if $H = 10\,\text{cm}$. This is the roughly in accord with the observed slumping scale of our salty cylinder as seen in Fig.7.16. We shall see in Chapters 8 and 9 that $L_\rho \sim 1000\,\text{km}$ in the atmospheric troposphere and $L_\rho \sim 30\,\text{km}$ in the main thermocline of the ocean; the respective deformation radii set the horizontal scale of the ubiquitous eddies observed in the two fluids.

7.3.5 Thermal wind in pressure coordinates

Eqs.(7.16) pertain to an incompressible fluid such as water or the ocean. The thermal wind relation appropriate to the atmosphere is untidy when expressed with height as a vertical coordinate (because of ρ variations). However it becomes simple when expressed in pressure coordinates. To proceed in p coordinates, we write the hydrostatic relation:

$$\frac{\partial z}{\partial p} = -\frac{1}{g\rho}$$

[10] In a stratified fluid the buoyancy frequency (Section 4.4) is given by $N^2 = -\frac{g}{\rho}\frac{d\rho}{dz}$ or $N^2 \sim \frac{g'}{H}$ where $g' = g\frac{\Delta\rho}{\rho}$ and $\Delta\rho$ is a typical variation in density over the vertical scale H.

and take, for example, the p-derivative of the x-component of Eq.(7.8) yielding:

$$\frac{\partial u_g}{\partial p} = -\frac{g}{f}\frac{\partial^2 z}{\partial p \partial y} = -\frac{g}{f}\left(\frac{\partial}{\partial y}\left[\frac{\partial z}{\partial p}\right]\right)_p = \frac{1}{f}\frac{\partial}{\partial y}\left(\frac{1}{\rho}\right)_p .$$

Since $1/\rho = RT/p$, its derivative *at constant pressure* is

$$\frac{\partial}{\partial y}\left(\frac{1}{\rho}\right)_p = \frac{R}{p}\left(\frac{\partial T}{\partial y}\right)_p ,$$

whence

$$\left(\frac{\partial u_g}{\partial p},\ \frac{\partial v_g}{\partial p}\right) = \frac{R}{fp}\left(\left(\frac{\partial T}{\partial y}\right)_p , -\left(\frac{\partial T}{\partial x}\right)_p\right). \tag{7.24}$$

Eq.(7.24) expresses the *thermal wind relationship* in pressure coordinates. By analogy with Eq.(7.8), just as height contours on pressure surface act as a streamlines for the geostrophic flow, then we see from Eq.(7.24) that temperature contours on a pressure surface act as streamlines for the thermal wind shear. We note in passing that one can obtain a relationship similar to Eq.(7.24) in height coordinates (see Q9 at end of Chapter), but it is less elegant because of the ρ factors in Eq.(7.4). The thermal wind can also be written down in terms of potential temperature; see Q10, also at the end of the Chapter.

The connection between meridional temperature gradients and vertical wind shear expressed in Eq.(7.24), is readily seen in the zonal-average climatology — see Figs.5.7 and 5.20. Thus, since temperature decreases poleward, $\partial T/\partial y < 0$ in the northern hemisphere, but $\partial T/\partial y > 0$ in the southern hemisphere; hence $f^{-1}\partial T/\partial y < 0$ in both. Then Eq.(7.24) tells us that $\partial u/\partial p < 0$: so, with increasing height (decreasing pressure), winds must become increasingly eastward (westerly) in both hemispheres (as sketched in Fig.7.19), which is just what we observe in Fig.5.20.

The atmosphere is also close to thermal wind balance on the large scale at any instant. For example Fig.7.20 shows T on the 500 mbar surface on 12GMT on June 21st, 2003, the same time as the plot of the 500 mbar height field shown in Fig.7.4. Remember that by Eq.(7.24), the T contours are streamlines of the geostrophic shear, $\frac{\partial \mathbf{u}_g}{\partial p}$. Note the strong meridional gradients in middle latitudes associated with the strong meandering jet stream. These gradients are also evident in Fig.7.21, a vertical cross section of temperature, T, and zonal wind, u, through the atmosphere at 80°W extending

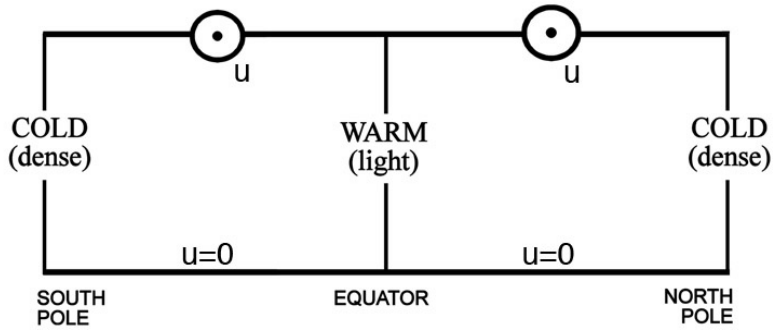

Figure 7.19: A schematic of westerly winds observed in both hemispheres in thermal wind balance with the equator-to-pole temperature gradient. (See Eq.(7.24) and the observations shown in Figs.5.7 and 5.20.)

from 20°N to 70°N at the same time as in Fig.7.20. The vertical coordinate is pressure. Note that, in accord with Eq.(7.24), the wind increases with height where T surfaces slope upward toward the pole and decreases with height where T surfaces slope downwards. The vertical wind shear is very strong in regions where the T surfaces steeply slope; the vertical wind shear is very weak where the T surfaces are almost horizontal. Note also the anomalously cold air associated with the intense low at 80°W, 40°N marked in Fig.7.4.

In summary, then, Eq.(7.24) accounts quantitatively, as well as qualitatively, for the observed connection between horizontal temperature gradients and vertical wind shear in the atmosphere. As we shall see in Chapter 9, an analogous expression of thermal wind applies in exactly the same way in the ocean too.

7.4 Subgeostrophic flow: the Ekman layer

Before returning to our discussion of the general circulation of the atmosphere in Chapter 8, we must develop one further dynamical idea. Although the large-scale flow in the free atmosphere and ocean is close to geostrophic and thermal wind balance, in boundary layers where fluid rubs over solid boundaries or when the wind directly drives the ocean, we observe marked departures from geostrophy due to the presence of the frictional terms in Eq.(6.29).

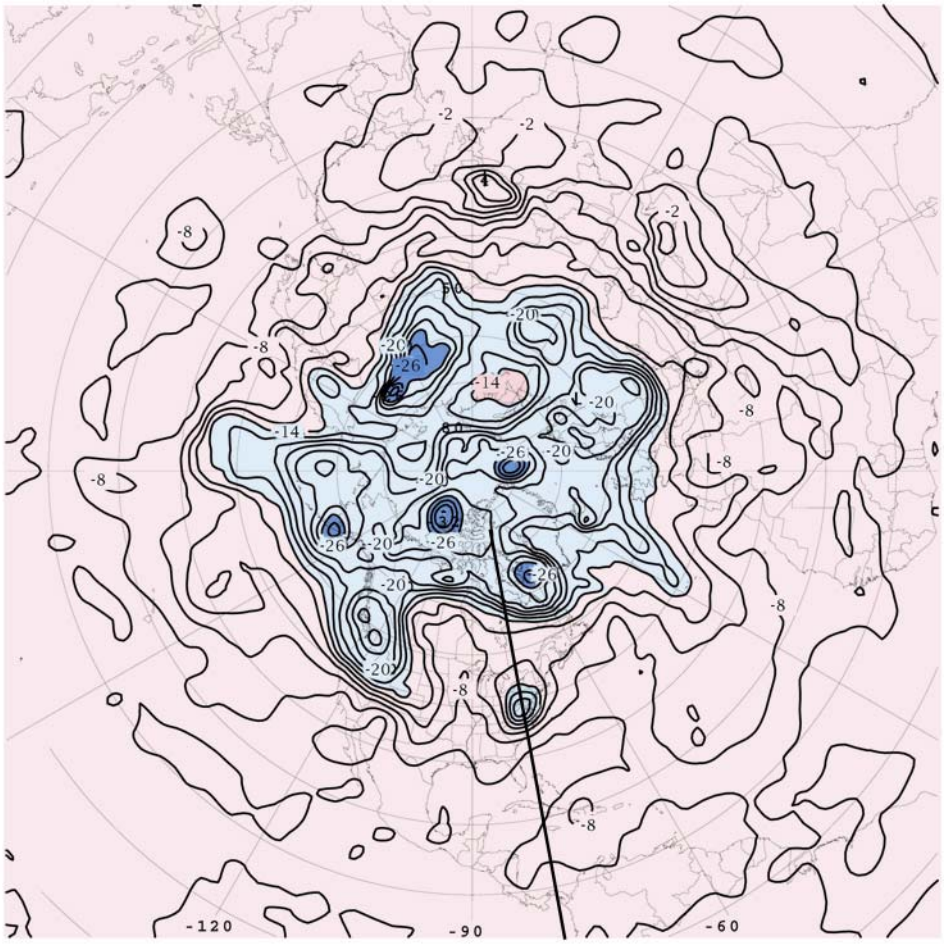

Figure 7.20: The temperature, T, on the 500 mbar surface at 12GMT on June 21st, 2003, the same time as Fig.7.4. The contour interval is 2 °C. The thick black line marks the position of the meridional section shown in Fig.7.21 at 80°W extending from 20°N to 70°N. A region of pronounced temperature contrast separates warm air (pink) from cold air (blue). The coldest temperatures over the pole get as low as −32 °C.

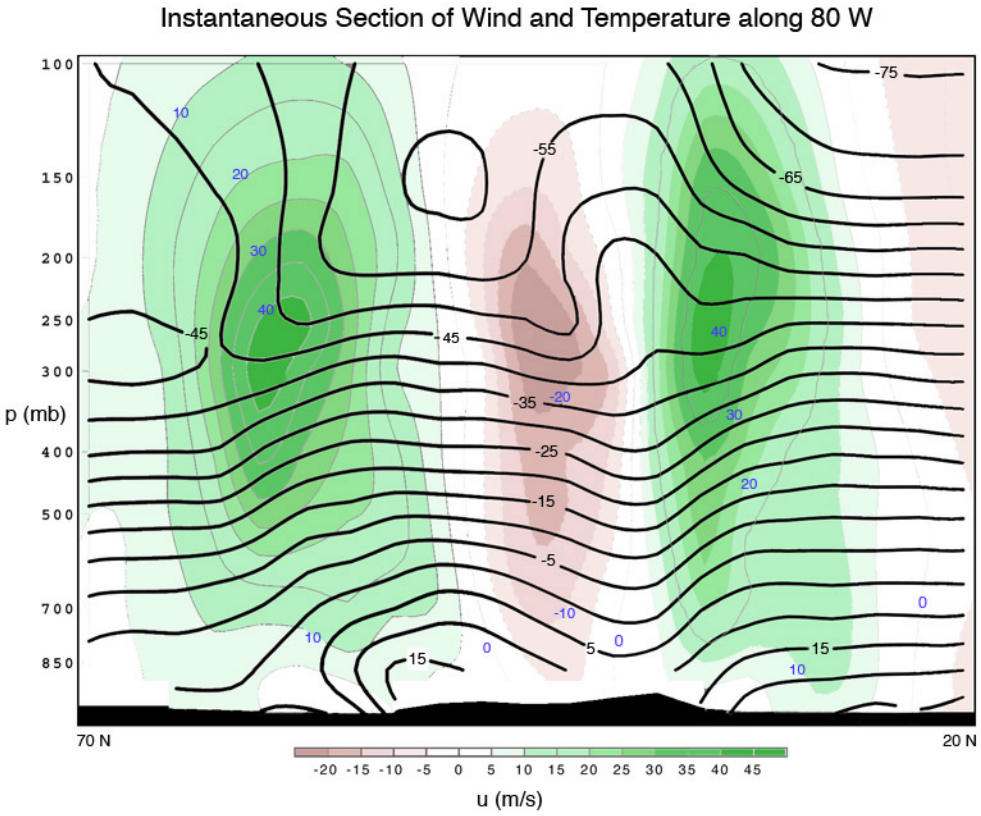

Figure 7.21: A cross section of zonal wind, u (color-scale, green indicating away from us and brown toward us) and thin contours every $5\,\mathrm{m\,s^{-1}}$), and potential temperature, T (thick contours every $5\,^{\circ}\mathrm{C}$) through the atmosphere at 80°W extending from 20°N to 70°N on June 21st, 2003 on at 12GMT, as marked on Figs.7.20 and 7.4. Note that $\frac{\partial u}{\partial p} < 0$ in regions where $\frac{\partial T}{\partial y} < 0$ and visa-versa.

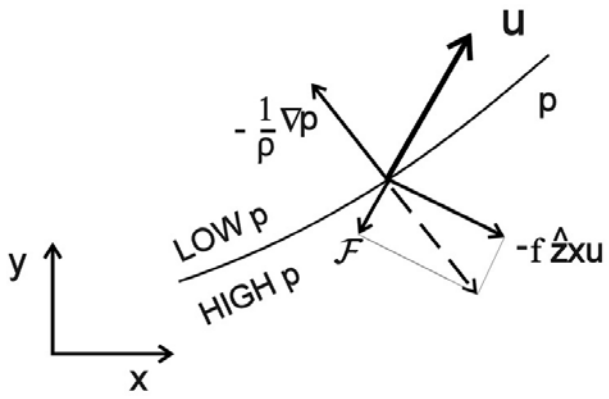

Figure 7.22: The balance of forces in Eq.(7.25): the dotted line is the vector sum $\mathcal{F} - f\widehat{\mathbf{z}} \times u$ and is balanced by $-\frac{1}{\rho}\nabla p$.

The momentum balance Eq.(7.2) pertains if the flow is sufficiently slow ($Ro << 1$) and frictional forces $\mathcal{F}$ sufficiently small — i.e. when both $\mathcal{F}$ and $D\mathbf{u}/Dt$ in Eq.(6.43) can be neglected. Frictional effects are indeed small in the interior of the atmosphere and ocean, but they become important in boundary layers. In the bottom kilometer or so of the atmosphere, the roughness of the surface generates turbulence which communicates the drag of the lower boundary to the free atmosphere above. In the top one hundred meters or so of the ocean the wind generates turbulence which carries the momentum of the wind down in to the interior. The layer in which $\mathcal{F}$ becomes important is called the 'Ekman layer' after the famous Swedish oceanographer who studied the wind-drift in the ocean, as will be discussed in detail in Chapter 10.

If the Rossby number is again assumed to be small but $\mathcal{F}$ is now *not* negligible, then the horizontal component of the momentum balance, Eq.(6.43), become:

$$f\widehat{\mathbf{z}} \times \mathbf{u} + \frac{1}{\rho}\nabla p = \mathcal{F} \tag{7.25}$$

To visualize these balances, consider Fig.7.22. Let's start with $\mathbf{u}$: the Coriolis force per unit mass, $-f\widehat{\mathbf{z}} \times \mathbf{u}$, must be to the right of the flow, as shown. If the frictional force per unit mass, $\mathcal{F}$, acts as a 'drag' it will be directed opposite to the prevailing flow. The sum of these two forces

is depicted by the dashed arrow. This must be balanced by the pressure gradient force per unit mass, as shown. Thus, the pressure gradient is no longer normal to the wind vector, or (to say the same thing) the wind is no longer directed along the isobars. Although there is still a tendency for the flow to have low pressure on its left, there is now a (frictionally-induced) component down the pressure gradient (toward low pressure).

Thus we see that in the presence of $\mathcal{F}$, the flow speed is subgeostrophic (less than geostrophic) and so the Coriolis force (whose magnitude is proportional to the speed) is not quite sufficient to balance the pressure gradient force. Thus the pressure gradient force 'wins', resulting in an ageostrophic component directed from high to low pressure. The flow 'falls down' the pressure gradient slightly.

It is often useful to explicitly separate the horizontal flow, $\mathbf{u}_h$, in the geostrophic and ageostrophic components thus:

$$\mathbf{u}_h = \mathbf{u}_g + \mathbf{u}_{ag} \tag{7.26}$$

where $\mathbf{u}_{ag}$ is the *ageostrophic* current, the departure of the actual horizontal flow from its geostrophic value, $\mathbf{u}_g$, given by Eq.(7.3). Using Eq.(7.25), Eq.(7.26) and the geostrophic relation Eq.(7.2), we see that:

$$f\widehat{\mathbf{z}} \times \mathbf{u_{ag}} = \mathcal{F} \tag{7.27}$$

Thus the ageostrophic component is always directed 'to the right' of $\mathcal{F}$ (in the northern hemisphere).

We can readily demonstrate the role of Ekman layers in the laboratory as follows.

7.4.1 GFD Lab X - Ekman layers: frictionally-induced cross-isobaric flow

We bring a cylindrical tank filled with water up to solid-body rotation at a speed of 5 rpm, say. A few crystals of potassium permanganate are dropped into the tank — they leave streaks through the water column as they fall and settle on the base of the tank — and float paper dots on the surface to act as tracers of upper level flow. The rotation rate of the tank is then reduced by 10% or so. The fluid continues in solid rotation creating a cyclonic vortex (same sense of rotation as the table) implying, through the geostrophic relation, lower pressure in the center and higher pressure near the rim of the

tank. The dots on the surface describe concentric circles and show little tendency toward radial flow. However at the bottom of the tank we see plumes of dye spiral inward to the center of the tank at about 45° relative to the geostrophic current — see Fig.7.23, top panel. Now we increase the rotation rate. The relative flow is now anticyclonic with, via geostrophy, high pressure in the center and low pressure on the rim. Note how the plumes of dye sweep around to point outward — see Fig.7.23, bottom panel.

In each case we see that the rough bottom of the tank slows the currents down there, and induces cross-isobaric, ageostrophic, flow from high to low pressure, as schematized in Fig.7.24. Above the frictional layer — which, as mentioned above, is called the 'Ekman layer' (see Section 10.1) — the flow remains close to geostrophic.

7.4.2 Ageostrophic flow in atmospheric highs and lows

Ageostrophic flow is clearly evident in the bottom kilometer or so of the atmosphere where the frictional drag of the rough underlying surface is directly felt by the flow. For example Fig.7.25 shows the surface pressure field and wind at the surface at 12GMT on June 21st, 2003, at the same time as the upper level flow shown in Fig.7.4. We see that the wind broadly circulates in the sense expected from geostrophy, anticylonically around highs and cyclonically around the lows. But the surface flow also has a marked component directed down the pressure gradient, into the lows and out of the highs, due to frictional drag at the ground. The sense of the ageostrophic flow is exactly the same as that seen in GFD Lab X (cf. Fig.7.23 and Fig.7.24).

A simple model of winds in the Ekman layer

Eq.(7.25) can be solved to give a simple expression for the wind in the Ekman layer. Let us suppose that the $x-$axis is directed along the isobars and that the surface stress decreases uniformly throughout the depth of the Ekman layer from its surface value to become small at $z = \delta$, where δ is the depth of the Ekman layer such that

$$\mathcal{F} = -\frac{k}{\delta}\mathbf{u} \tag{7.28}$$

where k is a drag coefficient that depends on the roughness of the underlying surface. Note that the minus sign ensures that $\mathcal{F}$ acts as a drag on the flow.

Figure 7.23: Ekman flow in a low pressure system (top) and a high pressure system (bottom) revealed by permanganate crystals on the bottom of a rotating tank. The black dots are floating on the free surface and mark out circular trajectories around the center of the tank directed anticlockwise (top) and clockwise (bottom).

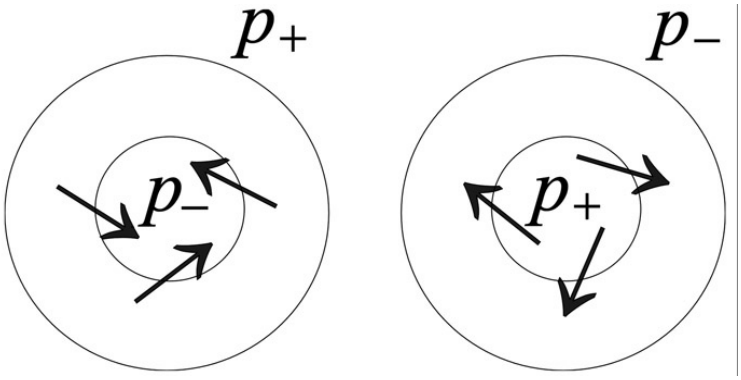

Figure 7.24: Flow spiralling in to a low pressure region (left) and out of a high pressure region (right) in a bottom Ekman layer. In both cases the ageostrophic flow is directed from high pressure to low pressure i.e. down the pressure gradient.

Then the momentum equations, Eq.(7.25), written out in component from along and across the isobars, become:

$$\begin{aligned} -fv &= -k\frac{u}{\delta} \\ fu + \frac{1}{\rho}\frac{\partial p}{\partial y} &= -k\frac{v}{\delta} \end{aligned} \tag{7.29}$$

Note that v is entirely ageostrophic, being the component directed across the isobars. But u has both geostrophic and ageostrophic components.

Solving Eq.(7.29) gives:

$$u = -\frac{1}{\left(1+\frac{k^2}{f^2\delta^2}\right)}\frac{1}{\rho f}\frac{\partial p}{\partial y};\ \frac{v}{u} = \frac{k}{f\delta} \tag{7.30}$$

Note that the wind speed is *less* than its geostrophic value and if $u > 0$, then $v > 0$ and *visa versa*; v is directed down the pressure gradient, from high to low pressure, just as in the laboratory experiment and in Fig.7.24.

In typical meteorological conditions, $\delta \sim 1\,\mathrm{km}$, k is between $(1 \longrightarrow 1.5) \times 10^{-2}\,\mathrm{m\,s^{-1}}$ and $\frac{k}{f\delta} \sim 0.1$. So the wind speed is only slightly less than geostrophic, but the wind blows across the isobars at an angle of some 6 to 12°. The cross-isobaric flow is strong over land (where k is large) where the friction layer is shallow (δ small) and at low latitudes (f small). Over

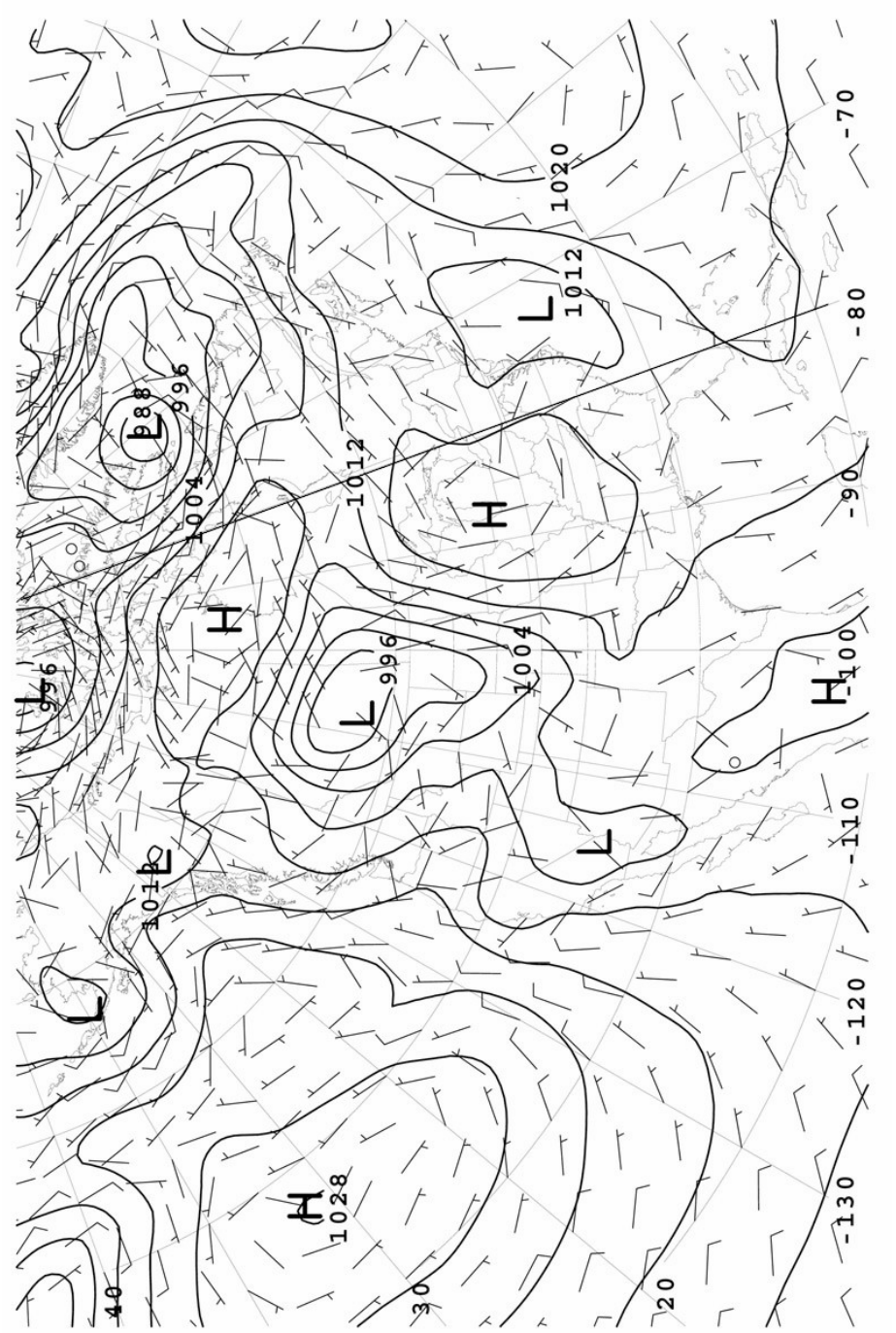

Figure 7.25: Surface pressure field and wind at the surface at 12GMT on June 21st, 2003, at the same time as the upper level flow shown in Fig.7.4. The contour interval is 4 mbar. One full quiver represents a wind of $10\,\mathrm{m\,s^{-1}}$; one half quiver a wind of $5\,\mathrm{m\,s^{-1}}$. The thick black lines marks the position of the meridional section shown in Fig.7.21 at 80°W.

the ocean, where k is small, the atmospheric flow is typically much closer to its geostrophic value than over land.

Ekman developed a theory of the boundary layer in which he set $\mathcal{F} = \mu \frac{\partial^2 \mathbf{u}}{\partial z^2}$ in Eq.(7.25) where μ was a constant eddy viscosity. He obtained what are now known as 'Ekman spirals' in which the current spirals from its most geostrophic to its most ageostrophic value (as will be seen in Section 10.1 and Fig.10.5). But such details depend on the precise nature of $\mathcal{F}$, which in general is not known. Qualitatively, the most striking and important feature of the Ekman layer solution is that the wind in the boundary layer has a component directed toward lower pressure; this feature is independent of the *details* of the turbulent boundary layer.

Vertical motion induced by Ekman layers

Unlike geostrophic flow, ageostrophic flow is not horizontally non-divergent; on the contrary, its divergence drives vertical motion because, in pressure coordinates, Eq.(6.12) can be written (if f is constant, so that geostrophic flow is horizontally non-divergent):

$$\nabla_p \cdot \ \mathbf{u}_{ag} + \frac{\partial \omega}{\partial p} = 0$$

This has implications for the behavior of weather systems. Fig.7.26 shows schematics of a cyclone (low pressure system) and an anticyclone (high pressure system). In the free atmosphere, where the flow is geostrophic, the wind just blows around the system, cyclonically around the low and anticyclonically around the high. Near the surface in the Ekman layer, however, the wind deviates toward low pressure, inward in the low, outward from the high. Because the horizontal flow is convergent into the low, mass continuity demands a compensating vertical outflow. This *Ekman pumping* produces ascent — and, in consequence, cooling, clouds and possibly rain — in low pressure systems. In the high, the divergence of the Ekman layer flow demands subsidence (through *Ekman suction*): high pressure systems tend to be associated with low precipitation and clear skies.

7.4.3 Planetary-scale ageostrophic flow

Frictional processes also play a central role in the atmospheric boundary layer on planetary scales. Fig.7.27 shows the annual average surface pressure field

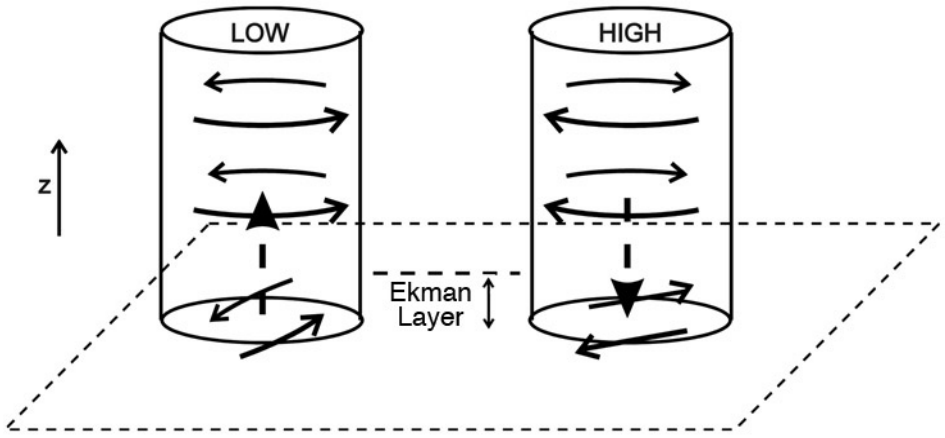

Figure 7.26: Schematic diagram showing the direction of the frictionally-induced ageostrophic flow in the Ekman layer induced by low pressure and high pressure systems. There is flow in to the low inducing rising motion (the dotted arrow) and flow out of a high inducing sinking motion.

in the atmosphere, p_s. We note the belt of high pressure in the subtropics (latitudes $\pm 30°$) of both hemispheres, more or less continuous in the southern hemisphere, confined in the main to the ocean basins in the northern hemisphere. Pressure is relatively low at the surface in the tropics and at high latitudes ($\pm 60°$), particularly in the southern hemisphere. These features are readily seen in the zonal-average p_s shown in the top panel of Fig.7.28.

To a first approximation, the surface wind is in geostrophic balance with the pressure field. Accordingly (see the top and middle panels of Fig.7.28) since $\frac{\partial p_s}{\partial y} < 0$ in the latitudinal belt between 30° and 60°N, then from Eq.(7.4), $u_s > 0$ and we observe westerly winds there; between 0° and $30°N$, p_s increases, $\frac{\partial p_s}{\partial y} > 0$ and we find easterlies, $u_s < 0$ — the trade winds. A similar pattern is seen in the southern hemisphere (remember $f < 0$ here); note the particularly strong surface westerlies around 50°S associated with the very low pressure observed around Antarctica in Fig.7.27 and 7.28 (top panel).

Because of the presence of friction in the atmospheric boundary layer, the surface wind also shows a significant ageostrophic component directed from high pressure to low pressure. This is evident in the bottom panel of Fig.7.28 which shows the zonal average of the meridional component of the surface wind, v_s. This panel shows the surface branch of the meridional flow

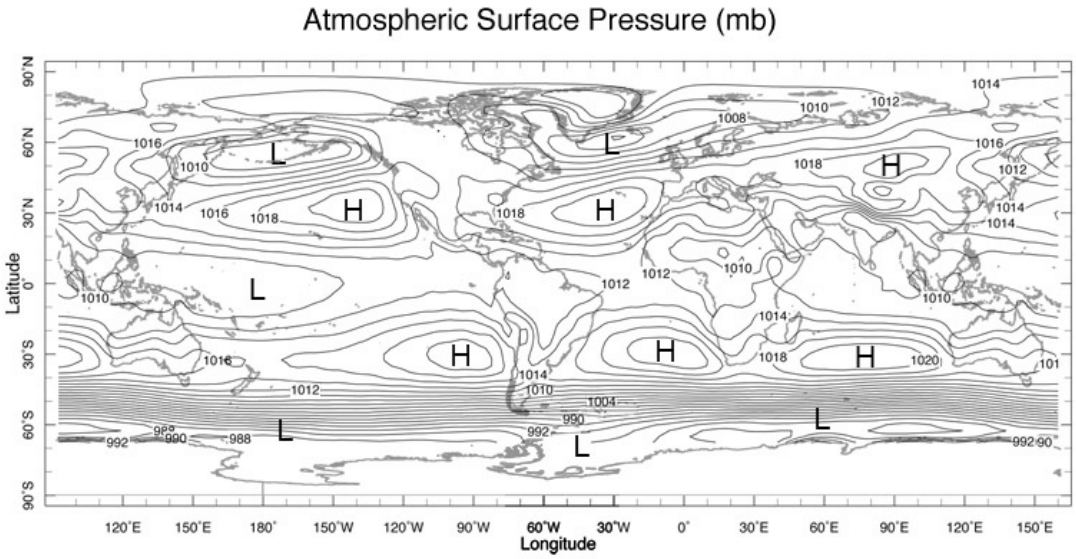

Figure 7.27: The annual-mean surface pressure field in mbar with major centers of high and low pressure marked. The contour interval 5 mbar.

in Fig.5.21 (top panel). Thus in the zonal average we see v_s, which is entirely ageostrophic, feeding rising motion along the inter-tropical convergence zone at the equator, and being supplied by sinking of fluid in to the subtropical highs of each hemisphere around $\pm 30°$, consistent with Fig.5.21.

We have now completed our discussion of balanced dynamics. Before going on to apply these ideas to the general circulation of the atmosphere and, in subsequent chapters, of the ocean, we summarize our key equations in Table 7.1.

7.5 Problems

1. Define a streamfunction ψ for non-divergent, two-dimensional flow in a vertical plane:

$$\frac{\partial u}{\partial x} + \frac{\partial v}{\partial y} = 0$$

and interpret it physically.

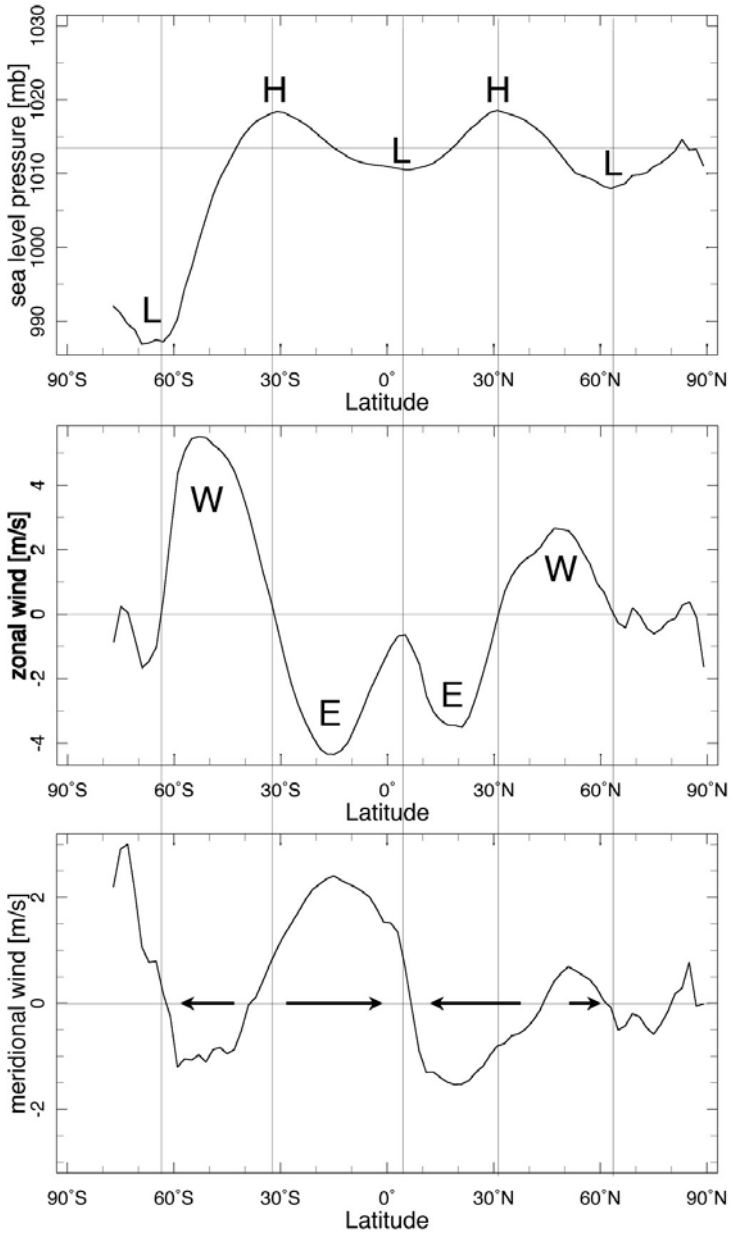

Figure 7.28: Anually and zonally averaged (top) sea level pressure in mbar, (middle) zonal wind in $\mathrm{m\,s^{-1}}$, and (bottom) meridional wind in $\mathrm{m\,s^{-1}}$. The horizontal arrows mark the sense of the meridional flow at the surface.

(x, y, z) coordinates	(x, y, z) coordinates	(x, y, p) coordinates
$\nabla \equiv \left(\frac{\partial}{\partial x}, \frac{\partial}{\partial y}, \frac{\partial}{\partial z}\right)$	$\nabla \equiv \left(\frac{\partial}{\partial x}, \frac{\partial}{\partial y}, \frac{\partial}{\partial z}\right)$	$\nabla_p \equiv \left(\frac{\partial}{\partial x}, \frac{\partial}{\partial y}, \frac{\partial}{\partial p}\right)$
general	(incompressible — OCEAN)	(comp. perfect gas — ATMOS)
Continuity		
$\frac{\partial \rho}{\partial t} + \nabla \cdot (\rho u) = 0$	$\nabla \cdot u = 0$	$\nabla_p \cdot u = 0$
Hydrostatic balance		
$\frac{\partial p}{\partial z} = -g\rho$	$\frac{\partial p}{\partial z} = -g\rho$	$\frac{\partial z}{\partial p} = -\frac{1}{g\rho}$
Geostrophic balance		
$fu = \frac{1}{\rho}\widehat{z} \times \nabla p$	$fu = \frac{1}{\rho_{ref}}\widehat{z} \times \nabla p$	$fu = g\widehat{z}_p \times \nabla_p z$
Thermal wind balance		
	$f\frac{\partial u}{\partial z} = -\frac{g}{\rho_{ref}}\widehat{z} \times \nabla \sigma$	$f\frac{\partial u}{\partial p} = -\frac{R}{p}\widehat{z}_p \times \nabla T$

Table 7.1: **Summary of key equations.** Note that (x, y, p) is not a right-handed coordinate system. So while $\widehat{\mathbf{z}}$ is a unit vector point toward increasing z, and therefore upward, $\widehat{\mathbf{z}}_p$ is a unit vector point toward decreasing p — and therefore also upward.

Show that the instantaneous particle paths (streamlines) are defined by $\psi = \text{const}$, and hence in steady flow the contours $\psi = \text{const}$ are particle trajectories. When are trajectories and streamlines not coincident?

2. What is the pressure gradient required to maintain a geostrophic wind at a speed of $v = 10\,\mathrm{m\,s^{-1}}$ at $45°N$? In the absence of a pressure gradient show that air parcels flow around circles in an anticyclonic sense of radius $\frac{v}{f}$.

3. Draw schematic diagrams showing the flow, and the corresponding balance of forces, around centers of low and high pressure in the midlatitude southern hemisphere. Do this for:

   (a) the geostrophic flow (neglecting friction), and

   (b) the subgeostrophic flow in the near-surface boundary layer.

4. Consider a low pressure system centered on 45°S, whose sea level pressure field is described by

$$p = 1000\mathrm{hPa} \; - \Delta p \; e^{-r^2/R^2} \; ,$$

   where r is the radial distance from the center. Determine the structure of the geostrophic wind around this system; find the maximum geostrophic wind, and the radius at which it is located, if $\Delta p = 20\mathrm{hPa}$, and $R = 500\mathrm{km}$. [Assume constant Coriolis parameter, appropriate to latitude 45°S, across the system.]

5. Write down an equation for the balance of radial forces on a parcel of fluid moving along a horizontal circular path of radius r at constant speed v (taken positive if the flow is in the same sense of rotation as the earth).

   Solve for v as a function of r and the radial pressure gradient and hence show that:

   (a) if $v > 0$, the wind speed is less than its geostrophic value,

   (b) if $|v| << fr$ then the flow approaches its geostrophic value and

   (c) there is a limiting pressure gradient for the balanced motion when $v > -\frac{1}{2}fr$.

Comment on the asymmetry between clockwise and anticlockwise vortices.

6. (i) A typical hurricane at, say, 30° latitude may have low-level winds of $50\,\mathrm{m\,s^{-1}}$at a radius of 50 km from its center: do you expect this flow to be geostrophic?

   (ii) Two weather stations near 45°N are 400 km apart, one exactly to the northeast of the other. At both locations, the 500 mbar wind is exactly southerly at $30\,\mathrm{m\,s^{-1}}$. At the north-eastern station, the height of the 500 mbar surface is 5510 m; what is the height of this surface at the other station?

   What vertical displacement would produce the same pressure difference between the two stations? Comment on your answer. You may take $\rho_s = 1.2\,\mathrm{kg\,m^{-3}}$.

7. Write down an expression for the centrifugal acceleration of a ring of air moving uniformly along a line of latitude with speed u relative to the earth, which itself is rotating with angular speed Ω. Interpret the terms in the expression physically.

   By hypothesizing that the relative centrifugal acceleration resolved parallel to the earth's surface is balanced by a meridional pressure gradient, deduce the geostrophic relationship

$$fu + \frac{1}{\rho}\frac{\partial p}{\partial y} = 0$$

   (in our usual notation and where $dy = a d\varphi$).

   If the gas is perfect and in hydrostatic equilibrium, derive the thermal wind equation.

8. The vertical average (with respect to log pressure) of atmospheric temperature below the 200 mbar pressure surface is about 265 K at the equator and 235 K at the winter pole. Calculate the equator-to-winter-pole height difference on the 200 mbar pressure surface, assuming surface pressure is 1000 mbar everywhere. Assuming that this pressure surface slopes uniformly between 30° and 60° latitude and is flat else-

where, use the geostrophic wind relationship (zonal component) in pressure coordinates,

$$u = -\frac{g}{f}\frac{\partial z}{\partial y}$$

to calculate the mean eastward geostrophic wind on the 200 mbar surface at 45° latitude in the winter hemisphere. Here $f = 2\Omega \sin\varphi$ is the Coriolis parameter, g is the acceleration due to gravity, z is the height of a pressure surface and $dy = a \times d\varphi$ where a is the radius of the earth is a northward pointing coordinate.

9. From the pressure coordinate thermal wind relationship, Eq.(7.24), and approximating

$$\frac{\partial u}{\partial p} \simeq \frac{\partial u/\partial z}{\partial p/\partial z} \ ,$$

show that, in geometric height coordinates,

$$f\frac{\partial u}{\partial z} \simeq -\frac{g}{T}\frac{\partial T}{\partial y}.$$

The winter polar stratosphere is dominated by the "polar vortex," a strong westerly circulation at about 60° latitude around the cold pole, as depicted schematically in Fig.7.29. (This circulation is the subject of considerable interest, as it is within the polar vortices—especially that over Antarctica in southern winter and spring—that most ozone depletion is taking place.)
Assuming that the temperature at the pole is (at all heights) 50 K colder at 80° latitude than at 40° latitude (and that it varies uniformly in between), and that the westerly wind speed at 100 mbar pressure and 60° latitude is $10\,\mathrm{m\,s^{-1}}$, use the thermal wind relation to estimate the wind speed at 1 mbar pressure and 60° latitude.

10. Starting from Eq.(7.24), show that the thermal wind equation can be written in terms of potential temperature thus:

$$\left(\frac{\partial u_g}{\partial p}, \ \frac{\partial v_g}{\partial p}\right) = \frac{1}{\rho\theta}\left(\left(\frac{\partial\theta}{\partial y}\right)_p, -\left(\frac{\partial\theta}{\partial x}\right)_p\right).$$

11. Fig.7.30 shows, schematically, the surface pressure contours (solid) and mean 1000 mbar − 500 mbar temperature contours (dashed), in the

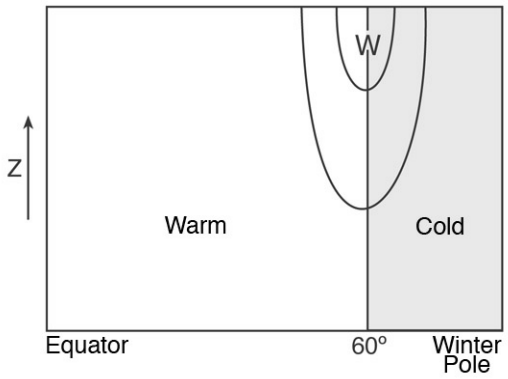

Figure 7.29: A schematic of the winter polar stratosphere dominated by the "polar vortex," a strong westerly circulation at $\sim 60^\circ$ around the cold pole.

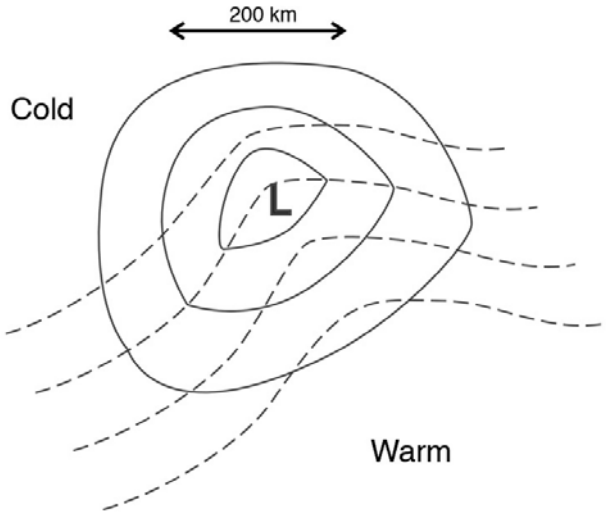

Figure 7.30: A schematic of surface pressure contours (solid) and mean $1000\,\mathrm{mbar} - 500\,\mathrm{mbar}$ temperature contours (dashed), in the vicinity of a typical northern hemisphere depression (storm).

vicinity of a typical northern hemisphere depression (storm). "L" indicates the low pressure center. Sketch the directions of the wind near the surface, and on the 500 mbar pressure surface. (Assume that the wind at 500 mbar is significantly larger than at the surface.) If the movement of the whole system is controlled by the 500 mbar wind (i.e., it simply gets blown downstream by the 500 mbar wind), how do you expect the storm to move? [Use density of air at 1000 mbar $= 1.2\,\mathrm{kg\ m^{-3}}$; rotation rate of Earth $= 7.27 \times 10^{-5}\,\mathrm{s^{-1}}$; gas constant for air $= 287\,\mathrm{J\ kg^{-1}}$.]